Hindawi
Journal of Chemistry
Volume 2023, Article ID 7891518, 27 pages
https://doi.org/10.1155/2023/7891518

Review Article

A Review on Cassava Residues as Adsorbents for Removal of Organic and Inorganic Contaminants in Water and Wastewater

Vasu Gajendiran,[1] **Prabu Deivasigamani**,[1] **Selvaraju Sivamani**,[2] **and Ponnurengam Malliappan Sivakumar**[3,4]

[1]*School of Bio and Chemical Engineering, Sathyabama Institute of Science and Technology, Chennai, India*
[2]*Engineering Department, University of Technology and Applied Sciences, Salalah, Oman*
[3]*Institute of Research and Development, Duy Tan University, Da Nang, Vietnam*
[4]*School of Medicine and Pharmacy, Duy Tan University, Da Nang, Vietnam*

Correspondence should be addressed to Prabu Deivasigamani; dprabhu78@gmail.com and Ponnurengam Malliappan Sivakumar; sivamedchem@gmail.com

Received 21 September 2022; Revised 4 November 2022; Accepted 24 November 2022; Published 26 April 2023

Academic Editor: Mahmoud Nasr

An increase in water demand for drinking, agriculture, and industries necessitates the treatment of water and wastewater. Among various conventional treatment techniques available, adsorption is found to be one of the most economical and feasible methods. Adsorbents from plant biomass are effective for the removal of organic and inorganic pollutants. Cassava has gained attention among researchers during the past decades due to its plentiful availability and resilient characteristics. Even though cassava contains cyanogenic glucosides as toxins, it is used in industries for development of various products. Cassava stem, rhizome, peel, and bagasse are industrial residues that are generated in abundance. The present review focusses on factors affecting adsorption using cassava residues, adsorbent preparation and activation methods, equilibrium, mass transfer, kinetics, and thermodynamic studies of adsorption.

1. Introduction

According to the Food and Agricultural Organization (FAO), cassava is considered to be one of the significant crops in the tropical region of the world [1]. The cassava plant consists of leaves and tubers as feed and food, respectively, and stem and rhizome being nonedible parts [2]. Cassava-producing industries generate peel and bagasse as residues and utilize the pulp to produce starch, flour, chips, and bioethanol [3]. The production statistics of cassava tubers reveal an average production of 268, 283.8, and 293.5 MMT during 2011–13, 2014–16, and 2018–20, respectively, with a sharp decline in 2017 at 277 million tons (Figure 1). As production increased during the mentioned periods, cassava-producing industries emerged as a promising sector for economic growth [4]. Hence, the waste generated from cassava-producing industries requires a suitable alternate option for waste to wealth conversion. Adsorbents could be the potential route for utilization of cassava peel, bagasse, stem, and rhizome.

Adsorption is an exothermic process in which liquid, dissolved solid, or gas atoms, ions, or molecules (adsorbate) accumulate inside the top surface of another solid substance (adsorbent) [5]. Adsorption is caused by an imbalance of forces forming hydrogen, Van der Waals, covalent, and ionic bonds among the two species, the adsorbent and the adsorbate [6]. Adsorption is used in chemical process industries for sugar refining, wastewater treatment, chromatography, gas purification, moisture removal, metallurgy, etc. [7]. The advantages of adsorption include operating in mild conditions and having simpler designs. Conventional methods are available to treat wastewater, but adsorption creates interest among researchers due to its economics [8, 9].

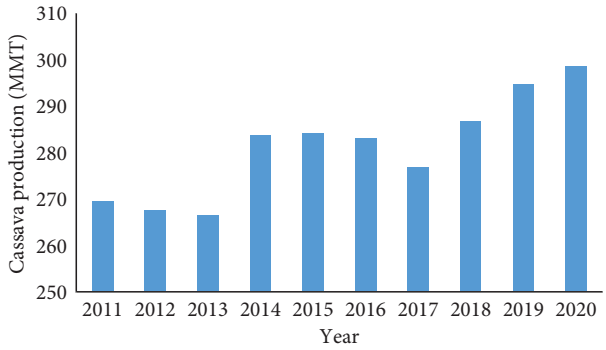

Figure 1: Cassava production in the world from 2011 to 2020 (FAOSTAT, 2021).

In the literature, various parts of cassava are reported to be adsorbents used in the removal of heavy metals, for example, zinc ([10–13]), copper ([11, 13–21]), lead ([20–28]), cobalt ([29, 30]), vanadium [30], chromium ([13, 17, 30, 31]), and cadmium ([12, 15, 32–34]), dyes such as rhodamine B [35], direct red [36], methylene blue ([36–40]), methyl orange [40], and reactive dyes [41], antibiotics ([22, 42–44]), phosphorous [45], biodiesel purification [46], organic pollutants from industrial effluents ([29, 47, 48]), and free fatty acid [49]. In addition, ZnO nanoparticles synthesized from cassava starch are used as adsorbents [50].

The present review highlights various activation methods, process parameters, isotherms, kinetics, thermodynamics, and binding mechanisms of adsorption using cassava-based adsorbents.

2. Factors Affecting Adsorption

Adsorption can be affected by various factors such as pH, initial concentration of adsorbates, contact time, adsorbent dosage, adsorbent size, and temperature, in addition to agitation speed (Figure 2). The process optimization of the aforementioned factors is required to maximize outcomes of adsorption, percentage removal, and adsorption capacity, the latter being the predominant.

2.1. Effect of pH. In the study of the adsorption process, the parameter pH is critical as the degree of electrostatic charges given by ionized adsorbates is controlled by it. As a result, the rate of adsorption varies with the medium pH, not in a particular pattern. At low pH, the adsorption capacity for anionic molecules generally increases, whereas it decreases for cationic molecules [51]. The electrostatic repulsion between the positively charged adsorbate and the adsorbent surface diminishes when the pH of the medium elevates, resulting in a rise in charge density of surfaces [52].

By adjusting the pH between 3 and 6, Belcaid et al. [7] examined the impact of pH on the process of chromium and cobalt removal from the solution by cassava peel carbon. They discovered that, in acidic environments, H^+ ions protonate the carbon surface of the cassava peel, favouring the electrostatic interaction between $HCr_2O_7^{-2}$ and the positively charged surface while creating competition

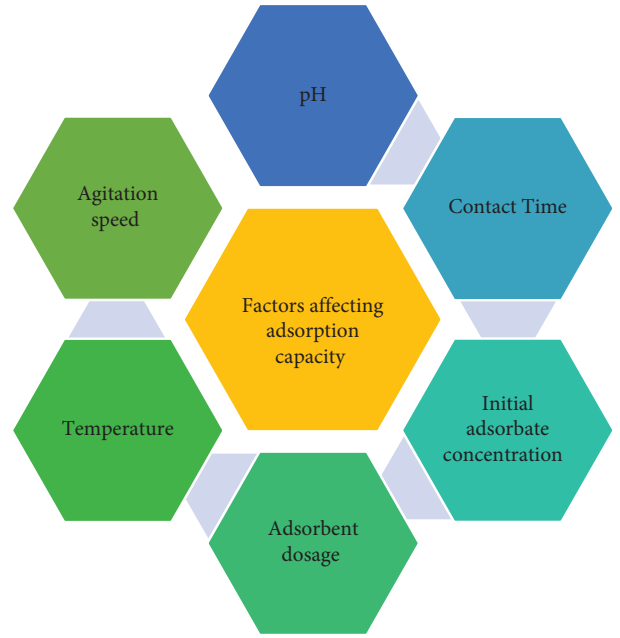

Figure 2: Factors affecting adsorption capacity.

between H^+ ions and CO_2^+ ions for the adsorption site. They discovered that a pH of 3 is ideal for removing chromium and a pH of 6 for removing cobalt.

Beakou et al. varied the pH from 3 to 9 to investigate the impact of pH on the cassava rind carbon's ability to remove malachite green, which is a pigment, from an aqueous solution [53]. They discovered that the adsorption of malachite green increases noticeably at pH levels that correspond to those of primary malachite green solutions. The quantity of malachite green absorption marginally rises in the ideal basic pH zone. It is possible that negative electrostatic forces will help the process of adsorption (surface charges change by means of cationic dye malachite green and cassava rind carbon). Because H^+ ions participate with cationic malachite green for the same adsorption sites at pH levels below 6.98, malachite green absorption is minimal.

Kurniawan et al. calculated the outcome of pH variation on Ni(II) ion uptake from an aqueous solution by fluctuating pH from 1 to 9 [5]. The findings demonstrate that the quantity of Ni(II) ion absorption rises gradually as pH rises from 1 to 5, peaking at pH 4.5. Compared to pH 4.5, less Ni(II) is adsorbed at higher pH levels. The occurrence of metal hydroxide [$Ni(OH)_2$], which occurs at alkali pH ranges ($pH > 7$), may be the origin of this phenomenon. Ni(II) ions are less concentrated in the solution due to the production of $Ni(OH)_2$, and as a result, less Ni(II) is removed by the cassava peel. Because of this, a pH of 4.5 is chosen for biosorption of metal investigations and helps as the ideal means for Ni(II) elimination.

2.2. Effect of Contact Time. According to equilibrium analysis, adsorption capacity increases as the contact time increases to a point, after which further increase in the contact time does not increase adsorbate uptake on

adsorbent due to saturation. The quantity of the adsorbate desorbing from the adsorbent present in the solution and the quantity of the adsorbate being adsorbed onto the adsorbent are in dynamic equilibrium. The time to establish this condition is known as the equilibrium time, and the quantity of the adsorbate adsorbed at that time represents the maximal adsorption capacity of the adsorbent under the operating conditions [54]. The contact time between adsorbents and adsorbates has a substantial impact on adsorption performance.

Abia et al. studied the outcome of time on adsorption of cadmium on thioglycolic acid-modified cassava fibre by changing the contact time from 5 to 30 minutes [55]. They found that the adsorption of cadmium was rapid at first 5 to 10 minutes and that adsorption capacity was achieved at 30 minutes. Also, they concluded that the faster rate of adsorption at the initial time of 5 to 10 minutes may be due to availability of uncovered active sites on the adsorbent surface.

Gunasekaran analysed the outcome of time for elimination of Metanil Yellow from an aqueous solution by using cassava peel and varying the time in the range of 0–1440 minutes [56]. He concluded that the percentage of Metanil Yellow dye removal increases rapidly with time but slows on attaining equilibrium. At the first 480 minutes of the contact time, the percentage dye slowly increased as availability of vacant sites on the adsorbent surface increased. At 480 minutes of the contact time, the Metanil Yellow dye reached an equilibrium state. At this stage, a dynamic equilibrium state between the amount of dye desorbing from the adsorbent and that being adsorbed on the adsorbent is established. After 960 minutes of the contact time, it started to decrease because of the saturation of active sites which do not allow further adsorption to take place.

Belcaid et al. [7] investigated the outcome of the contact time for elimination of chromium and cobalt from an aqueous solution by using cassava peel carbon and varying the time between 5 and 180 minutes. They discovered that there was rapid sorption uptake after 40 minutes of metal ion contact with activated carbon. Due to the nature of the accessible surface sites for the process of adsorption, the second stage is a sluggish phase of metal ion elimination that evolved from 50 min until 180 min. There are many sites available for sorption to take place when the interaction between the heavy metal ion and carbon from the cassava peel is established at the beginning of sorption, which accounts for the rapid metal ion uptake seen. The repulsive interactions between the already adsorbed metal ion and the entering sorbate and the constrained number of available sites for occupation cause the rate of subsequent adsorption to decrease as the uptake progresses, and the available sites are occupied.

2.3. Effect of Initial Adsorbate Concentration. The percentage removal increases and the adsorption capacity decreases with an increase in initial adsorbate concentrations. The effect of initial adsorbate concentrations is performed by preparing adsorbate solution at different concentrations using fixed pH, temperature, and contact time. The effect of initial adsorbate concentrations is used to study the interaction between adsorbates and adsorbents through isotherm models [57].

Hassan [58] studied the effect of initial dye concentrations on removal of malachite green dye from an aqueous solution by varying the concentration from 10 to 300 mg/L, and he found that maximum dye removal was achieved at a malachite green dye concentration of 100 mg/L.

By adjusting the quantity of 3 M H_3PO_4-activated cassava peel carbon from 10 to 50 mg/L, Thompson et al. [59] studied the impact of the initial lead ion concentration on the % removal and adsorption capabilities of lead ions from wastewater. They observed that as concentration increased, adsorption capacities increased, while % clearance decreased. This could be explained by the fact that there were initially few lead ions on the surface of adsorbents at lower concentrations, but as lead ion concentrations rose for a fixed number of sites and stayed constant, the number of substances that could be accommodated inside the diffusion layer enhanced, and the disposal of lead ions decreased. Cassava peels showed a maximum adsorption capacity of 27 mg/g at an initial concentration of 200 mg/g; however, with a preliminary concentration in the range of 50 mg/g, the adsorption capacity was 50.2 mg·g. With cassava peels, the highest clearance percentage of 89 was achieved at an initial concentration of 50 mg/g.

Ja'afar et al. [60] analysed the result of heavy metallic ion concentrations for adsorption elimination of copper ions from aqueous solvents by using amidoxime-modified polyacrylonitrile-grafted-cassava starch (AN-g-CS) and changing the preliminary concentration of cuprum ions at 25, 50, 75, 100, and 200 ppm, respectively. It validates that amidoxime-improved poly(AN-g-CS) increased and reached its saturation point at 100 ppm as the original volume per unit mass of cuprum ions (28 ppm) was raised up to 150 ppm.

Due to more widely accessible solutes as well as electrostatic interactions between solute and active sites, the adsorption capacity rose as the number of potential binding sites grew.

2.4. Effect of the Adsorbent Dosage. Adsorption capacity is calculated as the mass of the adsorbate removed per adsorbent mass. The rate of adsorption surges as the adsorbent dosage rises as a rise in the adsorbent dosage increases the number of sorption sites at the exterior of adsorbents. To study the consequence of the adsorbent dose on the process of adsorption, trials are executed by preparing different levels of mass of adsorbents at the fixed initial adsorbate concentration and equilibrium time [56].

Navya et al. [61] investigated the consequence of the adsorbent dosage for elimination of mixed responsive dye from simulated effluents using cassava trunk biochar adsorbents and by varying the adsorbent dosage from 0.6 g/l to 4.1 g/l. They discovered that the highest dye removal was 78 percent and that the adsorption capacity was 13.93 mg/g at an optimal concentration of 100 mg per 100 mL of dye solution.

Dos Santos et al. [62] studied the effect of the adsorbent dosage on removal of tartrazine yellow dye from the experimental solution by means of cassava waste biosorbents and by altering the dosage of adsorbents from 2.4 g/L to 12.4 g/L. They concluded that greater biosorbent concentrations encourage greater adsorption effectiveness. Adsorption was 35.8 percent at 0.1 at a dosage of 2.5 g/L, and efficiency improved to 83.3 percent at 0.1 at a concentration of 12.5 g/L. Therefore, there are a proportion of active sites that can be occupied by TAR molecules that have been adsorbed because the contact area increases with increasing biosorbent mass. A dose of 7.4 g/L was determined to be the most suitable for further studies since it is close enough to the border value and offers material savings.

Okorocha et al. [63] analysed the outcome of the adsorbent dosage for adsorptive elimination of crystal violet using raw cassava peels as adsorbents and by varying the adsorbent dosage. They noticed that, as the dosage of adsorbents rose, the removal effectiveness of the crystal violet dye also increased. This finding can be explained by the fact that, as the dosage of the adsorbent was raised, the quantity of active surface sites in pure cassava peel areas increased. Although the adsorption equilibrium capacity dropped with an increase in the adsorbent dosage, the percentage of crystal violet removal of dye rose. The accessibility of all active sites during the adsorption process may be limited because of duplication or agglomeration of the energetic or adsorption sites.

2.5. Effect of Temperature. Temperature affects the adsorption process based on the properties of bonds formed between adsorbate sites and adsorbents and the solubility of the adsorbate in the medium. At low temperature, adsorption due to strong and weak bonds increases, whereas it increases for strong bonds and decreases for weak forces [64].

Theng and Tan [65] investigated the outcome of temperature of the environment on the adsorption potential of one of the most reactive methylene blue dyes in addition to Congo red dye on powder of cassava leaf by changing the temperature within the range of 25°C to the extent of 75°C. They concluded that, as soon as the temperature improved from 25°C to 45°C, an increasing trend was seen for the removal rate of methylene blue dye (from 99.45% to 99.91%) because the frequency of collisions between the adsorbent and adsorbate (dye solution) increased at higher temperature, which promotes adsorption on the adsorbent surface. Only 98.95 percent removal was achieved at 75°C when the temperature was increased further to 50°C because the high temperature of the dye solution may have broken intermolecular hydrogen bonds between the dyes and the adsorbent, which are the key contributors to the adsorption process. The clearance rate of Congo red dye, on the other hand, showed a declining trend as the temperature was raised from 25 to 75 C (from 99.67 percent to 97.95 percent). This might be because a higher temperature results in more acidic pH. Congo red dye was more likely to dissolve in water under these very acidic conditions and was more challenging to remove from the solution.

By altering the temperature from 30°C to 50°C, Scheufele et al. [66] investigated the impact of temperature on the biological sorption of straight black dye on cassava root husks. They drew the conclusion that straight black dye sorption using the cassava root husk is by nature an exothermic process since larger yields of adsorption occurred at lower temperatures (30°C). However, only a very little change was seen for the elevated temperature (between 40 and 50°C).

Li et al. [67] investigated the consequence of temperature change for elimination of Congo red dye from an aqueous solution using cassava residue and by changing the temperature from 30°C to 50°C. They found that the adsorptive capacity did not vary markedly with an increase in temperature from 30°C to 50°C, indicating that energy gained or released through the process of adsorption was insignificant.

2.6. Effect of Adsorbent Size. Because of the greater surface area, the adsorption rate increases with decreasing particle diameter. The restriction to the adsorbate's penetration into the adsorbent resulting from internal diffusion as well as transfer of mass is lessened with smaller particle size. Due to this circumstance, equilibrium is reached more quickly, and the greatest amount of adsorption capacity is possible [7].

Tejada-Tovar et al. [68] investigated the outcome of particle size on hexavalent chromium adsorption from the experimental solution using cassava peels as an adsorbent with different sizes between 0.355 and 1 mm. They found that the highest amount of adsorbed metal ions on cassava peel biomass was achieved at the smallest particle size (0.355 mm). The particle size of adsorbent materials influences the adsorption process because the surface area is increased to carry out the transfer of different ions from a liquid phase to a solid phase. The number of heavy metal ions that can be adsorbed is directly proportional to volume, and it is well known that this volume is directly proportional to the surface area. In addition, there is a greater surface area for small particle size; hence, a greater number of pores per mass unit are available for uptake of heavy metal ions.

Using 0.3 M HNO_3-activated cassava peels as an adsorbent, Sulaiman et al. [69] investigated the impact of particle size on the adsorption of copper and zinc ions from an aqueous solution. They found that, compared to the size of mesh, 100 mesh (150 micron), and 80 mesh, 120 mesh size (125 micron) is generally more successful in absorbing copper (Cu^{2+}) and zinc (Zn^{2+}) metal ions (180 micron). This finding supports the notion that, due to a larger surface area of contact between the adsorbent and the adsorbate, the ability of the adsorbent increases with decreasing particle size.

Rubio et al. [70] investigated the consequence of size of the particle on deletion of methylene blue from the experimental solution by using raw cassava bark residue and acid- and alkali-modified cassava bark residue with different particle sizes from 20 to 400 mesh numbers. They discovered that the adsorption phenomena of methylene blue of 20 (88.0 percent), 30 (87.8 percent), and 40 were not significantly affected by particle size (88.4 percent). However, the

alkalinization of CBR led to a significant improvement, exhibiting 94.3 percent of methylene blue removal, while the acidification of CBR showed a minor drop in methylene blue separation (85.5 percent).

2.7. Effect of Mixing Speed. Horsfall and Abia [11] calculated the result of mixing speediness for adsorption of cadmium from an aqueous solution by using cassava waste biomass (tuber bark) and conducting the experiment with different speeds from 50 to 200 rpm. They concluded that the agitated samples showed a 35 percent increase in adsorption over the first 30 minutes of contact so that sorbate ions can effectively be transferred onto the sorbent surface by adequate interactions between metallic ions and biomass binding sites. The sorption efficiency was discovered to be marginally lower at 200 rotations per minute (rpm) than it was at 150 rpm. This finding might point to weak Van der Waals contacts between sorbents and chromium ions, which might be broken in the presence of intense turbulence. Therefore, an agitation speed is 150 rpm.

Ndlovu et al. [30] considered the consequence of agitation speeds on the deletion of cobalt, chromium, and vanadium from the experimental solution by using cassava-peel biomass (both raw/treated with thioglycolic acid). The agitation speed ranged from 50 to 200 rpm during the experiment. They discovered that, as the agitation speed rose from 50 to 150 rpm, there was an increase in sorption. This is such that the mass transfer rate of metal ions on the surface of the biomass is maximized as the agitation speed is increased. However, as the agitation speed increased from 150 to 200 rpm, sorption decreased. This happens when there is a break in the link between metal ions and adsorbents, which causes metal ions to desorb from the surface sites. The outcomes also suggest that physical adsorption, not chemical adsorption, is occurring.

Aulia et al. [71] examined the outcome of the mixing speed for the dye elimination from screen printing industry wastewater using cassava peels (20% H_2SO_4 acid activated) and by varying the speed of 50, 100, 150, 200, and 250 rpm. The researchers discovered that 100 rpm was the ideal stirring speed for removing colours, removing 96.78 percent. The adsorbate and the adsorbent were dispersed equally at the maximum speed and throughout the maximum contact duration, increasing the adsorption process.

Table 1 summarizes the effect of parameters on adsorption using cassava residues as adsorbents.

3. Preparation of Adsorbents and Activation Methods

The materials used for preparation of adsorbents are rich in carbon [74]. Among the plant biomass, lignocellulosic materials are more appropriate for adsorbent preparation. Lignocellulosic materials basically contain lignin, cellulose, and hemicellulose. Lignin is an organic polymer composed of coumaryl alcohol, sinapyl alcohol, and coniferyl alcohol. Cellulose is a homopolysaccharide that is composed of many units of glucose connected through β-1,6-glycosidic linkage. Hemicellulose is a heteropolysaccharide mainly comprises pentoses. Lignocellulosic materials rich in hemicellulose yield a less quantity of adsorbents, whereas materials rich in cellulose and lignin yield a high quantity of adsorbents. Lignocellulosic materials are either angiosperms (hardwood) or gymnosperms (softwood). Gymnosperms are rich in hemicellulose, and angiosperms are rich in cellulose.

The steps followed in adsorbent preparation are breaking of plant biomass to coarse particles and then to fine ones. Then, the fine particles are washed to remove debris and light particles, dried at around 100°C, and activated to produce effective adsorbents (Figure 3). The economics of adsorbent preparation are minimum so that the wastewater treatment by adsorption can be feasible. Pyrolysis at high temperatures for a short time is one of the feasible methods for adsorbent preparation as it avoids multiple steps ([75–81]). However, energy consumption is higher in pyrolysis. To overcome this problem, multistep drying followed by activation is recommended. Drying of materials reduces moisture, and activation increases porosity and surface areas.

Activation may be performed by using chemicals or other agents. It is performed by mixing the adsorbate and activating agents at a specific loading ratio and concentration of agents. The mixture is agitated at the explicit speed for definite time and temperature. Finally, the mixture is washed to remove excess activating agents and then dried to constant weight.

Cassava peel and bagasse are rich in starch, whereas cassava stem and rhizome are rich in cellulose based on the level of growth. Thioglycolic acid, sulphuric acid, reactive dye, potassium hydroxide, phosphoric acid, nitric acid, mercaptoacetic acid, sodium bicarbonate, sodium hydroxide, oxalic acid, citric acid, zinc chloride, hydrochloric acid, titanium dioxide, hydroxylamine hydrochloride, ammonium persulphate, hydrogen peroxide, ferric chloride, ferrous sulphate, silver nitrate, epichlorohydrin, pyridine, ethylenediaminetetraacetic acid, magnetite, zinc oxide, chloromethyl hydroxyquinoline are reported to be utilized as activating agents for cassava-based materials. Magnetite and titanium dioxide were used to improve the magnetic and photocatalytic properties of cassava substances.

Tejada-Tovar et al. [68] examined the removal of hexavalent chromium using raw cassava peel powder and by activating with citric acid. The percentage removal has been increased from 54.3% for raw powder to 56.2% for activated materials. Being a tricarboxylic acid, citric acid does not exhibit significant removal upon activation.

Rubio et al. [70] examined the consequence of acid and alkali activation on cassava bark residue particles of varied sizes. Mesh numbers 20, 30, and 40 were cast off to examine the outcome of particle sizes of cassava bark residue for the removal of methylene blue dye. Mesh number 20 produced significant dye removal of 88.5% against 87.7 and 88.8%, respectively, for mesh numbers 30 and 40. 0.1 M sulphuric acid and sodium hydroxide were used as activation agents to remove dye at 85.6 and 94.2%, respectively. 0.1 M sodium hydroxide was found to be an effective activating agent for cassava bark residue to remove methylene blue dye.

Table 1: Effect of parameters on adsorption using cassava residues as adsorbents.

Adsorbate	Adsorbent	pH	Time (min)	Dosage (g/L)	Initial concentration (ppm)	Temperature (K)	Agitation speed (rpm)	Particle size	Reference
Metal ions									
Chromium	Cassava peel carbon (CPC)	3–6 (3)	5–180	0.02	10–60 (10)	288.15–328.15 (328.15)	300	40–63 μm	[7]
Cobalt	Cassava peel carbon (CPC)	3–6 (6)	5–180	0.02	10–60 (10)	288.15–328.15 (318.15)	300	40–63 μm	[7]
Chromium	Cassava peel carbon	2–12 (6)	5–180 (40)	0.02	10–40 (35)	298	300	40–63 mm	[7]
Nickel	Cassava peel	1–9 (4.5)	30–60	0.1–10 (0.5)	200	333	200	125–750 mm	[5]
Lead	Cassava root husk	4	2	0.1	0.5	298	240	50 μm	[6]
Copper	Cassava root husk	4	25	1	0.5	298	240	50 μm	[6]
Chromium	Cassava peel modified by citric acid	2–6 (2)	120	0.5	100	298	150	0.355 nm	[68]
Mercury	Mod. cassava peel	6	10–330	0.5	25–100 (100)	298	150	0.355–0.5 mm	[72]
Dyes									
Malachite green	Cassava rind carbon (CRC)	3–9 (7)	180	5	150	298	300	40–63 μm	[73]
Metanil yellow	Cassava peel	3–10 (8)	30–1440 (480)	0.5–7 (3)	30–400 (125)	298	150	0.125–0.710 (0.125 mm)	[56]
Other pollutants									
Norfloxacin	Cassava dreg biochar BC 350, pyrolysis at 350 K	3–9 (6)	480	0.5	10	298	200	0.45 μm	[54]
Norfloxacin	Cassava dreg biochar BC 450, pyrolysis at 450 K	3–9 (6)	480	0.5	10	298	200	0.45 μm	[54]
Norfloxacin	Cassava dreg biochar BC 550, pyrolysis at 550 K	3–9 (6)	480	0.5	10	298	200	0.45 μm	[54]
Norfloxacin	Cassava dreg biochar BC 650, pyrolysis at 650 K	3–9 (6)	480	0.5	10	298	200	0.45 μm	[54]
Norfloxacin	Cassava dreg biochar BC 750, pyrolysis at 750 K	3–9 (6)	480	0.5	10	298	200	0.45 μm	[54]
Nitrate	Modified cassava straw	2–12 (7)	30	0.01–1.0 (0.2)	25–75 mg/dm^3	293	120	150–200 μm	[64]

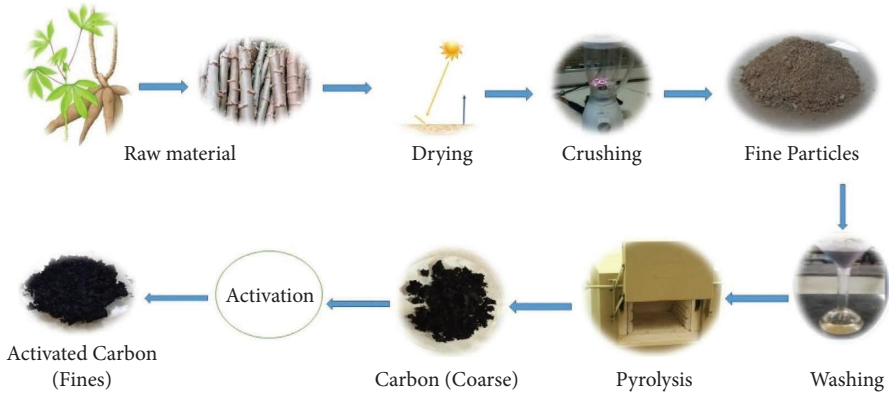

Figure 3: Preparation of adsorbents and activation methods.

Tri Widayati et al. [82] studied the removal of the total suspended solid present in batik liquid waste by using inactivated cassava peel carbon and activating carbon by 0.1 M hydrochloric acid and 1.0 M sodium hydroxide. They observed a decrease in the total suspended solid for the activating agent (hydrochloric acid) with an adsorption percentage of 47.83%, whereas with the activating agent (sodium hydroxide), the percentage of adsorption was 34.84%, and then, without the activating agent, the percentage of adsorption was found to be 28.57%.

Ndongo et al. [83] examined the synthesis and characterization of ferric chloride-activated cassava peel.

Table 2 summarizes several activation methods reported for adsorbent preparation from cassava residues.

4. Adsorption Isotherms

The adsorption isotherm is cast off to explain the interactions between adsorbates and adsorbents at the point of equilibrium [108] (Figure 4).

4.1. One-Parameter Isotherm Model

4.1.1. Henry's Isotherm Model. Henry's adsorption isotherm model is the most straightforward one since the partial pressure of the gas, which is being adsorbed, is proportional to the quantity of the surface adsorbate [109]. Henry's model offers an excellent fit for the sorption of the adsorbate at lower concentrations in most cases, while entire adsorbate substances are separated from one another. As a result, the following linear formula is used in Equation (1) to represent the concentrations of the used adsorbate in equilibrium conditions in the liquid phase (Ce) in addition to the adsorbed phases.

$$q_e = K_{HE} C_e, \tag{1}$$

where k_{HE} is Henry's constant.

4.2. Two-Parameter Isotherm Models

4.2.1. Langmuir Isotherm Model. The original purpose of this isotherm model for adsorption was to explain the sorption of gases onto solid-phase adsorbates, such as activated carbon. The process of molecules adhering to a solid surface, according to Langmuir, is centered on a kinetic concept in which there is continual bombarding of particles onto the surface and matching desorption or evaporating of particles from the interface with the zero rate of the accumulation at the substratum [110]. In other words, the rates of adsorption and desorption ought to be equal. The adsorption capabilities of various adsorbents have typically been evaluated and compared using the Langmuir isotherm model.

An empirical model called the Langmuir isotherm assumes that adsorbed coating is almost equal to one molecule level thick (monolayer adsorption) and that the process of adsorption takes place at equivalent, identical, and clearly localized spots. Even on adjacent sites, there should not be any sideway interaction or steric hindrance among the experimented adsorbed layer of molecules. This isotherm model presupposes that the phenomenon of adsorption is homogeneous and that separated molecules have sorption activation energy and constant enthalpies [111]. There should be no adsorbate migration in the superficial plane and equal adsorbate affinities at all sites. According to Langmuir theory, there is a connection between increasing distance and a sharp decline in attractive forces between molecules. The equation derived from the Langmuir isotherm can be improved for adsorption of an aqueous phase as given in the equation.

$$q_e = q_m \frac{K_L C_e}{1 + K_L C_e}, \tag{2}$$

where q_m and K_L are the maximum adsorption capacity and Langmuir constant, respectively.

The isotherm equation becomes Henry's law isotherm at small concentrations and low pressure. Pressure causes the amount of adsorbed material to increase linearly, and when the pressure is strong enough to cover a monolayer, the capacity of saturation of the quantity of adsorbed material is attained. Due to their strong attraction for one another, a greater affinity constant (b) results in extra surface exposure with the adsorbate particle [112]. The affinity constant decreases as the temperature (T) rises because the adsorption process is exothermal. For the adsorption

Table 2: Activation methods reported in the literature for adsorbent preparation from cassava residues.

Adsorbate	Adsorbent	Activation	Outcomes	Reference
Metal ions				
Cadmium	Thioglycolic acid-modified cassava fibre (MCF)	Chemical: 0.5 M and 1.0 M and thioglycolic acid modified	0.5 M MCF = 53.66% & 1.0 M MCF = 58.66%	[55]
Lead	Cellulose nanocrystal from cassava peel	Acid hydrolysis with 64% sulphuric acid	6.4 mg/g	[84]
Copper and zinc	Undyed cassava mesocarp (UDCM) and dyed cassava mesocarp (DCMI: 0.40 mm and DCMII: 0.63 mm)	Reactive dye	Copper: UDCP = 63 DCMI = 375.5 DCMII = 224/Zinc: UDCP = 12 DCMI = 34 DCMII = 21	[85]
Nickel	Activated carbon from cassava peel tubers	Alkali activation (87.9% KOH)/ACPH	51.81 mg/g	[51]
Nickel	Activated charcoal from cassava peel tubers	Acid activation (phosphoric acid 85%)/ACPA	51.86 mg/g	[51]
Nickel	Activated carbon from cassava peel tubers	Nonimpregnated carbon (NIC)	48.86 mg/g	[51]
Copper	Modified cassava fibre	Acid activation (0.3 M nitric acid) + 0.5 M mercaptoacetic acid-0.5 MCF	20.33%	[86]
Copper	Modified cassava fibre	Acid activation (0.3 M nitric acid) + 1.0 M mercaptoacetic acid-1.0 MCF	21.00%	[86]
Cadmium	Cassava starch-based super adsorbent polymer	Copolymerization	374.7 mg/g	[87]
Chromium	Cassava peel carbon (CPC)	Acid (phosphoric acid)/alkali ($NaHCO_3$)	166.33 mg/g	[7]
Cobalt	Cassava peel carbon (CPC)	Acid(phosphoric acid)/alkali ($NaHCO_3$)	301.63 mg/g	[7]
Chromium	Cassava peel carbon	Phosphoric acid (1 : 1) before carbonisation + 1% $NaHCO_3$ after carbonisation	166.35 mg/g	[7]
Cobalt	Cassava peel carbon	Phosphoric acid (1 : 1) before carbonisation + 1% $NaHCO_3$ after carbonisation	301.63 mg/g	[7]
Chromium	Cassava peel	1.5 M HNO_3	61.72%	[88]
Tartrazine	Cassava sievate	85% H_3PO_4 (1 : 1)	20.83 mg/g	[89]
Zinc	Cassava peel	HCl/0.5/1.0/1.5 M	7.8%/2.1%/1.1%	[90]
Copper	Cassava peel	HCl/0.5/1.0/1.5 M	298%/17.2%/18.4%	[90]
Iron	Cassava peel	HCl/0.5/1.0/1.5 M	55.4%/43.4%/61.4%	[90]
Lead	Cassava peel	HCl/0.5/1.0/1.5 M	80%/20%/100%	[90]
Zinc	Cassava peel	$ZnCl_2$/0.5/1.0/1.5 M	2.3%/2.6%/2.3%	[90]
Copper	Cassava peel	$ZnCl_2$/0.5/1.0/1.5 M	50.6%/60.5%/35.6%	[90]
Iron	Cassava peel	$ZnCl_2$/0.5/1.0/1.5 M	88%/89.1%/67.5%	[90]
Lead	Cassava peel	$ZnCl_2$/0.5/1.0/1.5 M	100%/100%/20%	[90]
Chromium	Cassava sludge-activated carbon	$ZnCl_2$ (sludge: $ZnCl_2$ ratio = 1 : 5)	98.22%	[91]
Lead	Cassava biomass modified with TiO_2 nanoparticles	TiO_2	99.84%	[92]
Nickel	Cassava biomass modified with TiO_2 nanoparticles	TiO_2	81.51%	[92]
Cadmium	Untreated cassava peel biomass/ acid-treated cassava peel biomass	0.5 M and 1.0 M thioglycolic acid treated	86.68 mg/g/647.48 mg/g	[11]
Zinc	Untreated cassava peel biomass/ acid-treated cassava peel biomass	0.5 M and 1.0 M thioglycolic acid treated	55.52 mg/g/559.74 mg/g	[11]
Cadmium	Unmodified cassava tuber bark/ acid-modified cassava tuber bark	0.5 M and 1.0 M thioglycolic acid treated	2.69 mg/g/11.48 mg/g/5.98 mg/g	[93]

Table 2: Continued.

Adsorbate	Adsorbent	Activation	Outcomes	Reference
Copper	Unmodified cassava tuber bark/ acid-modified cassava tuber bark	0.5 M and 1.0 M thioglycolic acid treated	11.48 mg/g/14.88 mg/g/28.49 mg/g	[93]
Zinc	Unmodified cassava tuber bark/ acid-modified cassava tuber bark	0.5 M and 1.0 M thioglycolic acid treated	11.48 mg/g/14.86 mg/g/37.88 mg/g	[93]
Copper from single-ion solution/wastewater	Unmodified cassava tuber bark/ acid-modified cassava tuber bark	1.0 M thioglycolic acid (ratio: 25 g : 250 ml)	Untreated: 71.3 mg/g acid treated: 85.2 mg/ g	[52]
Zinc from single-ion solution/wastewater	Unmodified cassava tuber bark/ acid-modified cassava tuber bark	1.0 M thioglycolic acid (ratio: 25 g : 250 ml)	Untreated: 43.4 mg/g acid treated: 58.1 mg/ g	[52]
Zinc	Cassava peel carbon	Impregnated with $ZnCl_2$	28%	[12]
Nickel	Cassava peel carbon	Impregnated with $ZnCl_2$	66.60%	[12]
Cadmium	Cassava peel carbon	Impregnated with $ZnCl_2$	50%	[12]
Copper	Modified cassava starch	Hydroxylamine hydrochloride	75.76 mg/g	[60]
Lead	Modified cassava stalk	EDTAD + Fe_3O_4	163.93 mg/g	[94]
Zinc	Modified cassava stalk	EDTAD + Fe_3O_4	84.74 mg/g	[94]
Pb/refinery wastewater	Unfermented cassava peel carbon	11.0 M $ZnCl_2$	95%	[95]
Cu/refinery wastewater	Unfermented cassava peel carbon	1.0 M $ZnCl_2$	80%	[95]
Fe/refinery wastewater	Unfermented cassava peel carbon	1.0 M $ZnCl_2$	70%	[95]
Pb/refinery wastewater	Fermented cassava peel carbon	1.0 M $ZnCl_2$	100%	[95]
Cu/refinery wastewater	Fermented cassava peel carbon	1.0 M $ZnCl_2$	94%	[95]
Fe/refinery wastewater	Fermented cassava peel carbon	1.0 M $ZnCl_2$	74%	[95]
Pb/refinery wastewater	Commercially activated carbon	1.0 M $ZnCl_2$	57%	[95]
Cu/refinery wastewater	Commercially activated carbon	1.0 M $ZnCl_2$	76%	[95]
Fe/refinery wastewater	Commercially activated carbon	1.0 M $ZnCl_2$	56%	[95]
Cadmium	Cassava peel biochar	300°C/activated by 1.63 M KOH	84%	[96]
Chromium	Cassava peel modified by citric acid	0.6 M citric acid	54% (raw) and 56% (citric acid modified)	[68]
Cadmium	Modified cassava peel	By 0.1 mol/L of NaOH (99%)	19.54 mg/g	[97]
Chromium	Modified cassava peel	By 0.1 mol/L of NaOH (99%)	42.46 mg/g	[97]
Chromium	Modified cassava peel	By 0.1 mol/L of H_2O_2 (36%)	43.97 mg/g	[97]
Copper	Grafted cassava starch	Grafting cassava starch with 5-chloromethyl-8-hydroxyquinoline	28.75 mg/g	[98]
Lead	Grafted cassava starch	Grafting cassava starch with 5-chloromethyl-8-hydroxyquinoline	46.512 mg/g	[98]
Copper	Cassava peel act. by 0.3 m HNO_3	Cassava peel act. by 0.3 m HNO_3	55.19%	[69]
Zinc	Cassava peel act. by 0.3 m HNO_3	Cassava peel act. by 0.3 m HNO_3	41.70%	[69]
Mercury	Mod. cassava peel	By 0.6 M citric acid	72.98%	[72]
Chromium	Cassava peel	Unmodified	54.33%	[68]
Chromium	Cassava peel	By 0.6 M citric acid	56.20%	[68]
Arsenic	Root husks of cassava nanoparticles loaded by using ZnO	ZnO	39.52 mg/g	[99]
Cadmium	Root husks of cassava nanoparticles loaded by using ZnO	ZnO	4205 mg/g	[99]
Lead	Root husks of cassava nanoparticles loaded by using ZnO	ZnO	44.27 mg/g	[99]
Chromium	Root husks of cassava nanoparticles loaded by using ZnO	ZnO	28.37 mg/g	[99]
Lead	Cassava peel carbon	2 M H_3PO_4	96.83%	[59]

Table 2: Continued.

Adsorbate	Adsorbent	Activation	Outcomes	Reference
Dyes				
Methylene blue	Modified cassava peel	Acid activation (phosphoric acid 85%)	99.98%/79.975 mg/g	[100]
Methylene blue	Cassava peel biochar	Acid activation (phosphoric acid 14%)	4.75 mg/g	[101]
Rhodamine B	Activated charcoal from cassava peel	Thermal (700°C)/chemical (phosphoric acid 1 : 1 ratio	100%/100%	[102]
Direct brown	Activated charcoal from cassava peel	Thermal (700°C)/chemical (phosphoric acid 1 : 1 ratio	10.35%/100%	[102]
Procion orange	Activated charcoal from cassava peel	Thermal (700°C)/chemical (phosphoric acid 1 : 1 ratio	5.3%/100%	[102]
Acid violet	Activated charcoal from cassava peel	Thermal (700°C)/chemical (phosphoric acid 1 : 1 ratio	83.0%/86.32%	[102]
Malachite green	Activated charcoal from cassava peel	Thermal (700°C)/chemical (phosphoric acid 1 : 1 ratio	100%/100%	[102]
Methylene blue	Activated charcoal from cassava peel	Thermal (700°C)/chemical (phosphoric acid 1 : 1 ratio	100%/100%	[102]
Naphthol blue black	Activated charcoal from cassava peel	Acid activation (60% phosphoric acid)	99.70%	[103]
Dye from printing industry wastewater	Activated charcoal from cassava peel	Acid activation (20% sulphuric acid)	96.78%	[71]
Malachite green	Cassava rind carbon (CRC)	Acid (phosphoric acid 1 : 1 ratio)/alkali (NaOH 1 M)	932.975 mg/g	[73]
Methylene blue	Cassava rind carbon (CRC)	Acid (phosphoric acid 1 : 1 ratio)/alkali (NaOH 1 M)	565 mg/g	[53]
Reactive red + Drimarene turquoise	Cassava stem biochar (CSB)	Acid/oxalic acid (1%)	88.40%	[61]
Sunset yellow	Cassava sievate	85% H_3PO_4 (1 : 1)	0.091 mg/g	[89]
Malachite green	Cassava peel carbon	Act. by (0.5 N $AgNO_3$)	93%	[8]
Malachite green	Cassava peel carbon	Act. by (H_2SO_4)	82.70%	[8]
Reactive dye	AC from cassava peel impregnates with $AgNO_3$/	AC from cassava peel impregnates with $AgNO_3$ (1%)/ 4 N H_2SO_4/4 N NaOH	90% ($AgNO_3$ impregnated)	[41]
Methylene blue	Cassava bark residue (raw/mod. H_2SO_4/ NaOH (20, 30, and 40 mesh size)	0.1 M H_2SO_4 and NaOH	88% (20 mesh no) 87.7% (30 mesh no) 88.5 (40 mesh no) 94.2% (alkali-activated 20 mesh no)	[70]
Methylene blue	Cassava leaf powder	By 95% ethanol	99.90%	[104]
Other pollutants				
Tartrazine	Cassava sievate	85% H_3PO_4 (1 : 1)	20.83 mg/g	[89]
Nitrate	Modified cassava straw	Epichlorohydrin and pyridine	2.14 mM/dm^3	[64]
Glucose	Carbon from cassava stems	KOH 1 : 2 w/w	3.33 mg/g	[105]
Cholesterol	Carbon from cassava stems	KOH 1 : 2 w/w	6.84 mg/g	[105]
COD/refinery wastewater	Unfermented cassava peel carbon	1.0 M $ZnCl_2$	64%	[95]
BOD/refinery wastewater	Unfermented cassava peel carbon	1.0 M $ZnCl_2$	83%	[95]
Phenol/refinery wastewater	Unfermented cassava peel carbon	1.0 M $ZnCl_2$	93%	[95]
COD/refinery wastewater	Fermented cassava peel carbon	1.0 M $ZnCl_2$	73%	[95]
BOD/refinery wastewater	Fermented cassava peel carbon	1.0 M $ZnCl_2$	86%	[95]
Phenol/refinery wastewater	Fermented cassava peel carbon	1.0 M $ZnCl_2$	96%	[95]
COD/refinery wastewater	Commercially activated carbon	1.0 M $ZnCl_2$	55%	[95]
BOD/refinery wastewater	Commercially activated carbon	1.0 M $ZnCl_2$	72%	[95]
Phenol/refinery wastewater	Commercially activated carbon	1.0 M $ZnCl_2$	83%	[95]
Nitrate	Cassava peel carbon	$ZnCl_2$ (1 : 1, 1 : 3 and 2 : 3)	81.6%(1 : 1 $ZnCl_2$)	[106]
Phenol	Cassava peel carbon act. by $ZnCl_2$	0.75 : 1 ($ZnCl_2$: cassava peel ratio)	16.67 mg/g	[107]
TSS of Bakaran batik	Cassava peel carbon	Raw	28.57%	[82]
TSS of Bakaran batik	Cassava peel carbon	0.1 M HCl	47.83%	[82]

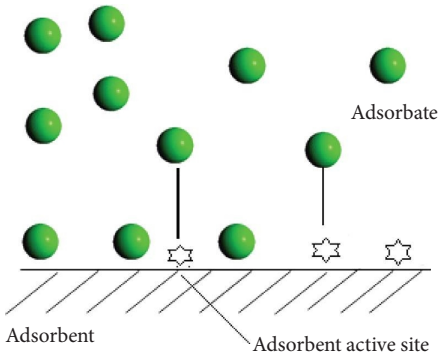

Figure 4: Adsorption isotherm explaining interactions between adsorbates and adsorbents.

procedure to take place, free energy (ΔG) reduces, and the reduction in the degrees of freedom is found to be negative conversion for the entropy (ΔS); thus, equation (3) is

$$\Delta H = \Delta G + T\Delta S < 0. \quad (3)$$

Enthalpy (H) negativity shows that heat was released throughout the adsorption process. Analogous to this, raising the heat of adsorption causes a rise in the quantity of surfactant adsorption, which means that the energy barrier for molecules to recover to the gas phase is larger. Because the molecules adsorbed require more energy to evaporate at higher temperatures, the amount of adsorbed material at a specific pressure falls as temperature increases.

Since sediments are in the form of heterogeneous adsorbents with dissimilar adsorption energies at every location, as well as the Langmuir model presumes a surface of homogeneous adsorbents with similar adsorption energies for each site, there are some shortcomings in the Langmuir isotherm model's explanation of how toxicant sediments facilitate adsorption. However, Henry's adsorption isotherm approach is thought to be the most straightforward one since the partial pressure of the adsorbing gas is proportional to the number of surface adsorbates, as per [109]. When all adsorbate molecules are kept apart from one another, Henry's model typically offers an excellent fit for the adsorption of adsorbates at small doses. Furthermore, the separation factor (R_L) is defined as a dimensionless constant which is represented in the equation.

$$R_L = \frac{1}{1 + K_L C_O}, \quad (4)$$

where C_o is the initial concentration of the adsorbate expressed in mg/L and K_L is the adsorption capacity expressed in mg/g. Variations in the appropriate area and the adsorbent's porosity can be associated with the K_L constant, suggesting that larger surface areas and pore volumes can lead to increased adsorption capacities. The separation factor reveals the kind of adsorption, which might be linear ($R_L = 1$), irreversible ($R_L = 0$), unfavourable ($R_L > 1$), or advantageous ($0 < R_L < 1$).

The Langmuir isotherm model fitted well for adsorption of malachite green by cassava rind carbon [53], cadmium, copper and zinc on cassava tuber bark [93], lead and zinc on modified cassava stalk [94], cadmium, zinc, and chromium on modified cassava peel, lead on grafted cassava starch [113], mixed dye of reactive red and Drimarene turquoise on cassava stem biochar [61], chromium, cobalt on cassava peel carbon [7], and ciprofloxacin on cassava dreg biochar at various pyrolysis temperatures ranging from 350–750 K [114].

4.2.2. Freundlich Isotherm Model. The Freundlich adsorption isotherm model describes the reversible cycle and the nonideal adsorption process. The Freundlich model, in contrast to the Langmuir isotherm model, is relevant to multilayer adsorption and is not restricted to monolayer creation. In this isotherm model, the heat of adsorption and affinities do not necessarily need to be distributed equally across the heterogeneous surface. The Freundlich isotherm model formulation defines surface heterogeneity and thus the exponential distribution of the active sites and active site energy [115]. For the adsorption of animal charcoal, the Freundlich isotherm adsorption concept was developed in the past. It demonstrated that, at different solution concentrations, the amount of solute that could be adsorbed on a given mass of a specific adsorbent was not constant.

The adsorbed amount in this instance is calculated by adding the amount of adsorption at each site. Stronger binding sites will first be occupied, and once the adsorption process is complete, the adsorption energy will begin to fall exponentially. The Freundlich isotherm model is now extensively cast off in heterogeneous irregular systems, for example, the adsorption of extremely interacting organic chemicals or species on molecular sieves or activated carbon. For systems with heterogeneous surfaces in the gas phase, this adsorption isotherm model is suitable. Due to this isotherm's inappropriate behaviour towards Henry's law at low pressure, it offers a constrained range of pressure. It does not have a finite limit when the pressure is high enough. This adsorption isotherm model therefore only applies to the limited amount of adsorption data. The nonlinearized form of the Freundlich model is given in the equation.

$$q_e = K_F C_e \frac{1}{n}. \quad (5)$$

The data of n, where K_F and n parameters are influenced by temperature, serve as an identifier of the type of isotherm. The strength of the adsorption process or heterogeneity of the surface, $1/n$, indicates the relative distribution of energy and the heterogeneity of the location of adsorbates. The adsorption process is favourable when $1/n$ is greater than zero ($0 < 1/n < 1$), unfavourable when $1/n$ is greater than 1, and irreversible when $1/n = 1$. The fact that pressure or concentration must drastically reduce to a low value prior to desorption of adsorbate molecules from the surface explains why the isotherm is irreversible [116].

The Freundlich isotherm model fitted well for adsorption of norfloxacin at various pyrolysis temperatures ranging from 350–750 K [54], nickel on cassava peel [5], and rhodamine on cassava slag carbon [57].

4.2.3. Dubinin–Radushkevich (D–R) Isotherm Model. For explaining the mechanism of adsorption with the distribution of Gaussian energy onto heterogeneous surfaces, the D–R adsorption isotherm model is typically utilized. The description of the adsorption of gases and vapours on microporous sorbents like activated carbon and zeolites typically uses this model. Due to the unrealistic asymptotic behaviour that is displayed, this model was successful in fitting the high solute activity and the intermediate adsorbate concentration range [117]. When pressure is low, the D–R isotherm model does not, however, predict Henry's law.

The D–R model is a semiempirical equation in contrast to Langmuir and Freundlich isotherm models, where the adsorption of this model follows the mechanism of pore filling. This model's underlying presumption is that it may be applied to physical adsorption processes and has a multilayer character that involves Van der Waals forces. This isotherm model is typically used to differentiate between the chemical and physical adsorption of metal ions. Temperature affects the D–R isotherm model. It is regarded as a defining and distinctive characteristic; as a result, when the potential energy square is plotted against the logarithm of the adsorbed amount, the appropriate data will form the characteristic curve, on which it is located. The D–R isotherm model has nonlinear form as given in the equation.

$$q_e = q_s e^{-K\varepsilon^2}. \tag{6}$$

In addition, where P_s is the saturation vapour pressure (atm) and P is the adsorbate equilibrium pressure (atm), the following equation can be used to calculate: (atm). A fundamental need for using the D–R isotherm model is accurately estimating the adsorption potential (ε). Following the adsorption of a unit of molar mass of the used adsorbate, it reflects the Gibbs free energy change of adsorbents. This isotherm model has been expanded to include the adsorption in the aqueous phase.

The Dubinin–Radushkevich isotherm model fitted well for adsorption of crystal violet on raw cassava peel [63] and mixed dye of reactive red and Drimarene turquoise on cassava stem biochar [61].

4.2.4. Temkin Isotherm Model. The Temkin empirical isotherm model was initially used to describe the chemisorption system known as hydrogen adsorption over platinum electrodes in an acidic solution. This isotherm model ignores extremely high and extremely low concentration values while considering the interaction between the adsorbent and the adsorbate. This model implies that, as surface coverage increases, the adsorption heat (H_{ads}) of all molecules in the layer drops linearly rather than logarithmically as a function of temperature [118]. Only an intermediate concentration range can be used with this adsorption isotherm model. Like the isotherm models presented above, the Temkin model has a nonlinear form as given in the equation.

$$q_e = \frac{RT}{b_T} \ln A_T C_e. \tag{7}$$

Both the A_{T} and b_T constants can be determined by displaying q_e vs. ln (C_e). This model is quite good at forecasting the equilibrium of the gas phase, assuming that it is not necessary for it to be arranged in a tightly packed structure with the same orientation. Its equation implies that binding energies are equally distributed. On the other hand, the presentation of complicated adsorption systems, such as aqueous phase adsorption isotherms, does not suit this isotherm model.

4.2.5. Flory–Huggins Isotherm Model. The solution theory of the Flory–Huggins equation provides a straightforward yet effective mathematical model for the thermodynamics of polymer mixtures. Entropy and enthalpy are combined to create the dissolution process, which may then be explained using the Flory–Huggins equation. According to this theory, solvent molecules occupy single sites, whereas polymer segments occupy lattice sites [119]. This premise allows for the calculation of the entropy of long-chain mixed compounds.

The kind and extent of the adsorbate's surface coverage on the adsorbent are considered by this isotherm adsorption model. Regarding the viability and spontaneity of the process, the Flory–Huggins isotherm model characterizes the nature of the adsorption process. The equation displays the nonlinear equations for this adsorption isotherm model. The parameters θ and C_o can be determined by using a nonlinear form as

$$\frac{\theta}{C_O} = F_{FH}(1-\theta)^{n_{FH}}. \tag{8}$$

In this context, n_{FH} stands for the number of metal ions that occupy the adsorption sites on two membranes and (θ) represents the degree of surface coverage. The adsorption equilibrium constant is K_{FH} as well. The spontaneous free Gibbs energy is typically calculated using it as it is related to the following expression:

$$\Delta G^o = -RT \ln K_{FH}. \tag{9}$$

4.2.6. Hill Isotherm Model. The requisite of various types of substrates which are homogeneous in nature is explained by the adsorption isotherm model. The adsorbate's capacity to attach at the single site on the surface of adsorbents may be impacting other binding sites on the same adsorbent, according to the isotherm model, which assumes that adsorption is a cooperative occurrence [120]. The nonlinear representation as well as the form of this isotherm model is stated as

$$q_e = \left[\frac{q_{SH} \cdot C_e^{nH}}{K_D + C_e^{nH}}\right]. \tag{10}$$

4.2.7. Halsey Isotherm Model. The multilayer adsorption system is evaluated by this adsorption isotherm, which also describes how it condenses at a significant distance from the

surface. Similar to the Freundlich isotherm model, the Halsey model is appropriate for multilayer adsorption and heterogeneous surfaces with nonuniformly distributed adsorption heat [121]. The nonlinearized form is

$$q_e = e^{\left(\ln K_H - \ln C_e\right)/n_H}, \tag{11}$$

where k_H and n_H are the Halsey constant and exponent, respectively.

4.2.8. Jovanovic Isotherm Model. The Langmuir isotherm model has all the underlying hypotheses for this model, plus the potential addition of mechanical contact between the molecules that are adsorbing and desorbing. The Jovanovic model's adsorption surface is taken into account, although its equation is frequently discared in physical analysis of adsorption for both mobile and single layer adsorption with no lateral interactions [122]. When the concentration is high, this model's equation can spread the saturation limit; once the concentration is small, Henry's law replaces it. The nonlinearization form is

$$q_e = q_{\max}\left(1 - e^{K_J C_e}\right), \tag{12}$$

where K_J is the Jovanovic constant (L/g).

4.2.9. BET (Brunauer–Emmett–Teller) Isotherm and Changed BET Isotherms. The equilibrium of gas-solid systems is where the Brunauer–Emmett–Teller hypothetical isotherm equation is utmost useful. The invention of the BET isotherm led to the creation of multiple layer adsorption schemes through comparative pressures between 0.06 and 0.34, which resemble a single-layer treatment between 0.5 and 1.50 [123]. This approach is frequently used to calculate the binding energy of the present state. The simplified form is given in Equation (13) as both C_{BET} and $C_{BET}(C_e/C_s)$ are greater than 1.

$$q_e = \frac{q_s}{1 - C_e/C_s}. \tag{13}$$

This model is prolonged towards the interface of liquid-solid, and it is designated as

$$q_e = \frac{q_{mBET} C_{BET} C_e}{\left(C_e - C_s\right)\left[1 + \left(C_{BET} - 1\right)C_e/C_s\right]}. \tag{14}$$

The BET model is regarded as a particular variety of the Langmuir model. With the addition of additional simplified assumptions, it incorporates the same fundamental assumptions as the Langmuir model; specifically, the second, third, and higher layers all contain the same adsorption energy. This energy is equivalent to the heat from fusion that is not predisposed by the connections among the localized adsorbent in addition to the adsorbate. The energy for the first layer, however, is distinct from that for the remaining layers. The number of layers goes to infinity when the concentration hits the saturation concentration.

4.3. Three-Parameter Isotherm Models

4.3.1. Redlich–Peterson Isotherm Model. This is a three-parameter amalgam isotherm model that combines the Freundlich and Langmuir isotherm models. This is not the phenomenon of single-layer adsorption because this model combines both concepts. The adaptable Redlich–Peterson isotherm model can be used in both heterogeneous and homogeneous systems. Both the denominator and the numerator of this isotherm model have an exponential function. The equilibrium of the adsorption onto a large range of concentrations is represented by its linear dependency on concentrations [124]. Since the numerator comes from the Langmuir isotherm model, it can get close to the Henry area at infinite dilution.

The nonlinear equation of this isotherm model is represented as

$$q_e = \frac{K_R C_e}{1 + a_R C_e^g}. \tag{15}$$

The expression of the reduced Freundlich model used in higher concentrations is given as

$$q_e = \frac{K_R}{a_R} C_e^{1-\beta}, \tag{16}$$

where $(1-\beta) = 1/n$ of the Freundlich isotherm model and $K_R/a_R = K_F$ are used. However, when $\beta = 1$, $a_R = b$, and $K_R = \text{bQ}\square$ it reduces to the Langmuir equation, and when $\beta = 0$ and Henry's constant is represented by $1/(1+b)$, it reduces to the Henry equation.

To solve the equations, this isotherm model uses a minimized approach. It increases the coefficient of correlation between the theoretical model's predictions and the data points from the experiment. Regarding the limitations, this model is consistent with the high concentration limit of the Freundlich isotherm model, where the exponent tends to be zero, and it approaches the ideal Langmuir condition at the low concentration limit when values are close to one.

The Redlich–Peterson isotherm model fitted well for adsorption of chromium and cobalt on cassava peel carbon [7] and methylene blue on cassava rind carbon [53].

4.3.2. Toth Isotherm Model. The objective of this type of isotherm model, an empirically changed version of the most familiar model derived from the Langmuir equation, is to lessen the predicted error between the data of the investigational result and the data predicted by the model. This isotherm model is mostly used to define the system of heterogeneous adsorption that fulfils equally small and large concentrations of adsorbates [125]. The nonlinear form of this isotherm model can be expressed as

$$q_e = \frac{K_T C_e}{\left(a_T + C_e\right)^{(1/t)}}. \tag{17}$$

When $t = 1$, the equation becomes the Langmuir isotherm equation. As a result, (t) is a parameter that represents the adsorption system's heterogeneity; the adsorption system is

regarded as heterogeneous when (t) is not equal to unity. Due to the independent relationship between temperature and the parameter t, the increasing temperature also causes a quick increase in a_T.

At low concentrations, the Toth equation simplifies to Henry's law, whereas at high concentrations, the Langmuir isotherm model approaches a finite capacity more slowly. This isotherm model is frequently used to describe the adsorption of different gases and vapours of organic substances. Additionally, the Toth isotherm model equation is seen as superior to the Sips equation in that it can describe the behaviour of the data at both high and low concentrations.

This isotherm model's slope has a constant limit at zero loading, but it begins to decline at given loading at a pace that is far faster than that of the Langmuir equation. This is explained by the heterogeneity's impact, which is reflected by the parameter t. Physically, molecules prefer to bind to high-energy sites, and as the adsorption process advances, molecules bind to locations with lower energies. This results in a slower increase in the adsorbed amount vs. pressure compared to that predicted by the Langmuir equation.

4.3.3. Sips Isotherm Model. The Sips isotherm model, which is derived to forecast the heterogeneity of adsorption systems and get over the restrictions connected with the rising concentrations of the adsorbate of the Freundlich model, was created by combining the Langmuir and Freundlich isotherm models. As a result, at high concentrations, an expression with a finite limit is created [126]. Without adsorbate-adsorbate interactions, the Sips model is valid for localizing adsorption. The Sips equation is given by the following nonlinear expression:

$$q_e = \frac{K_S C_e^{\beta} S}{1 + a_S C_e^{\beta} S}. \tag{18}$$

Due to the reduction to the Freundlich model at low adsorbate concentrations, the Sips isotherm model does not follow Henry's law. On the other hand, it predicts the monolayer adsorption characteristic of the Langmuir model at high adsorbate concentrations. The parameters in the equation are controlled by operating conditions like changes in temperature, pH, and concentration. Both the Freundlich and Sips models have the same drawbacks, in which they fail to provide the correct Henry's law limit when the pressure is low.

4.3.4. Khan Isotherm Model. This isotherm model, which represents both the Langmuir and Freundlich models, is a generalized model proposed for the adsorbate adsorption from pure solutions. This isotherm model was created for both single-component and multicomponent adsorption systems [127]. The equation of this model is expressed as

$$q_e = \frac{q_S b_K C_e S}{\left(1 + b_K C_e\right)^{a_K}}. \tag{19}$$

4.4. Four-Parameter Isotherm Models

4.4.1. Fritz–Schlunder Isotherm. Due to numerous coefficients in the isotherm, the Fritz–Schlunder isotherm is an empirical equation of the Langmuir–Freundlich type that can accommodate a variety of experimental results [128]. The equation of this isotherm model can be expressed as

$$q_e = \frac{q_{mFSS} K_{FS} C_e}{1 + q_m C_e^{MFS}}, \tag{20}$$

where MFS (the equilibrium model of Fritz–Schlunder) decreases to the Freundlich model for large adsorbate concentrations but becomes the Langmuir model if it is = 1. The isotherm parameters can be found via nonlinear regression analysis.

4.4.2. Baudu Isotherm Model. The Langmuir isotherm was compacted to the isotherm of Baudu as a result of the observation that determines the coefficients of the equation derived by Langmuir (b and q_m); using tangent measuring at different concentrations of the equilibrium reveals that these coefficients, which are derived from the equation, are not at all constants within the broader concentration range [129]. The selected range is between $(1 + x + y) < 1$ and $(1 + x) < 1$; this model is appropriate. When surface coverage is minimal, the Baudu-referred isotherm model is transformed into the isotherm model of Freundlich. To identify the parameters of this isotherm, the nonlinear regression investigation can be utilized in the equation as

$$q_e = \frac{q_m b_0 C_e^{1+x+y}}{1 + b_0 C_e^{1+x}}. \tag{21}$$

4.4.3. Weber–Van Vliet Isotherm Model. Weber and van Vliet projected an observed connection through four types of parameters to explain the equilibrium, which results in a variety of adsorption systems shown in the equation:

$$C_e = P_1 q_e^{\left(P_2 q_e^{P_3} + P_4\right)}, \tag{22}$$

where the isotherm parameters P_1, P_2, P_3, and P_4 are constants. The multiple nonlinear curve fitting method can predict the isotherm parameters by minimizing the summation of squares of residuals [130].

4.4.4. Marczewski–Jaroniec Isotherm Model. The four-parameter general Langmuir equation is another name for this isotherm model. The equation provides an expression for the isotherm equation as follows:

$$q_e = q_{MMJ} \left(\frac{\left(K_{MJ} C_e\right)^{nMJ}}{1 + C_e^{1+x+y}} \right)^{\left(M_{MJ}/n_{MJ}\right)}, \tag{23}$$

where n_{MJ} and M_{MJ} are variables describing the heterogeneity of the adsorbent surface. This isotherm model reduces to the Langmuir isotherm if n_{MJ} and M_{MJ} are both equal to 1

but to the Langmuir–Freundlich isotherm model if n_{MJ} and M_{MJ} are not equal. Based on the assumption of the local Langmuir isotherm model and the distribution of adsorption energy in the active sites on the adsorbent, this isotherm model is advised [131].

4.5. Five-Parameter Isotherm Models

4.5.1. Fritz–Schlunder Isotherm Model. A five-parameter observed model for the isotherm has been created that is considered to simulate model variations more accurately for use with a variety of equilibrium sets [128]. This isotherm model is expressed as

$$q_e = \frac{1_m FS_S K_1 C_e^{\alpha_{FS}}}{1 + K_2 C_e^{\beta_{FS}}}. \tag{24}$$

This model approaches the Langmuir isotherm model when α_{FS} and $\beta_{FS} = 1$, but it decreases to the Freundlich isotherm model for larger adsorbate concentrations.

The isotherm models for organic and inorganic pollutant adsorption in water and wastewater are listed in Table 3.

5. Adsorption Kinetics

Adsorption kinetics relate the adsorption rate to its capacity. The rate constant is directly related to the change in adsorption capacity with time.

5.1. Pseudofirst-Order (PFO) Model. The model of PFO was initially planned by the author of [132]. Equation (25) describes the PFO model's differential form [132]:

$$\frac{dq_t}{dt} = k_1 (q_e - q_t). \tag{25}$$

Integration in Equation (25), for the settings of $q_0 = 0$, produces Equation (26) as follows:

$$q_t = q_e\left(1 - e^{-k_1 t}\right). \tag{26}$$

The nonlinear technique, which can give precise model parameter estimates, is described in the section that follows. The equilibrium adsorption amount planned by the PFO model is the PFO parameter q_e. How quickly the adsorption equilibrium is reached is typically expressed using the PFO parameter k_1. On the other hand, Equation (1) demonstrates that the adsorption rate d_{qt}/dt is connected to both k_1 and $(q_e - q_t)$. When adsorption is sluggish, it is possible to achieve large values of $(q_e - q_t)$ and small values of k_1. To describe the adsorption rate with greater accuracy, the PFO rate presented in Equation (27) should be calculated rather than the values of k_1.

$$\text{PFOrate} = k_1 (q_e - q_t). \tag{27}$$

5.2. Pseudosecond-Order (PSO) Model. The adsorption process of lead upon peat was first modelled using the PSO model (Ho and McKay [133]). The PSO model was then widely used to explain the adsorption processes. In most published publications, the adsorption experimental values were predicted using the PSO model, and the rate constants of adsorption were calculated using the equation as follows:

$$\frac{dq_t}{dt} = k_2 (q_e - q_t)^2. \tag{28}$$

The integrated PSO model is described as

$$q_t = \frac{q_e^2 k_2 t}{1 + q_e k_2 t}. \tag{29}$$

The following part offers the nonlinear approach to resolving the PSO model. The PSO rate constant k_2 is being used to characterize the rate of adsorption equilibrium in a manner like that of the PFO rate constant k_1. However, both k_2 and $(q_e - q_t)^2$ are related to the adsorption rate, dq_t/dt. As a result, using the equation to compute the PSO rate is more accurate.

$$\text{PSOrate} = k_2 (q_e - q_t)^2. \tag{30}$$

5.3. Mixed-Order (MO) Model. The mixed-order (MO) model is considered in the form as

$$\frac{dq_t}{dt} = k_1' (q_e - q_t) + k_{21}' (q_e - q_t)^2. \tag{31}$$

The PFO and PSO rates for the MO model are calculated as

$$\text{PSOrate}' = k_1' (q_e - q_t), \tag{32}$$

$$\text{PSOrate}' = k_{21}' (q_e - q_t)^2. \tag{33}$$

The steps of diffusion and adsorption on active sites are typically described by the PFO rate and PSO rates, respectively. The MO model also depicts the entire adsorption process. The following requirements are necessary for the MO model's assumption to be met: (1) arbitrary adsorption stage, (2) either diffusion or adsorption serves as the rate-regulating phase, and (3) arbitrary initial concentration of the adsorbate in solution [91].

5.4. Elovich Model. The Elovich model's fundamental presumptions were as follows: (1) the activation energy increased with adsorption time and (2) the adsorbent surface was heterogeneous. An empirical model without clear physical implications is the Elovich model. The chemisorption of gas onto material is frequently modelled using this technique. The Elovich model has been described as follows [134]:

$$\frac{dq_t}{dt} = ae^{-bq_t}. \tag{34}$$

Integrating Equation (34), for the condition of $q_0 = 0$, yields Equation (35) as follows:

Table 3: Isotherm models reported in the literature for adsorption of organic and inorganic contaminants.

Adsorbate	Adsorbent	Adsorption isotherm	Reference
Metal ions			
Chromium	Cassava peel carbon (CPC)	Redlich–Peterson	[7]
Cobalt	Cassava peel carbon (CPC)	Redlich–Peterson	[7]
Chromium	Cassava peel carbon	Langmuir, Redlich–Peterson	[7]
Cobalt	Cassava peel carbon	Langmuir, Redlich–Peterson	[7]
Cadmium	Unmodified cassava tuber bark/acid-modified tuber bark of the specimen cassava	Langmuir	[93]
Copper	Unmodified cassava tuber bark/acid-modified tuber bark of the specimen cassava	Langmuir	[93]
Zinc	Unmodified cassava tuber bark/acid-modified tuber bark of the specimen cassava	Langmuir	[93]
Lead	Modified cassava stalk	Langmuir	[94]
Zinc	Modified cassava stalk	Langmuir	[94]
Nickel	Cassava peel	Freundlich	[5]
Cadmium	Modified cassava peel activated by 0.1 mol/L of 36% H_2O_2/98% H_2SO_4/99% NaOH	Langmuir	[97]
Lead	Modified cassava peel activated by 0.1 mol/L of 36% H_2O_2/98% H_2SO_4/99% NaOH	Langmuir	[97]
Chromium	Modified cassava peel activated by 0.1 mol/L of 36% H_2O_2/98% H_2SO_4/99% NaOH	Langmuir	[97]
Lead	Grafted cassava starch	Langmuir	[113]
Lead	Cassava peel carbon		[59]
Dyes			
Malachite green	Cassava rind Carbon (CRC)	Langmuir	[73]
Methylene blue	Cassava rind Carbon (CRC)	Redlich–Peterson	[53]
Reactive red + Drimarene turquoise	Cassava stem biochar (CSB)	Langmuir, Dubinin–Radushkevich	[61]
Crystal violet	Raw cassava peel powder	Dubinin–Radushkevich	[63]
Rhodamine B	Cassava slag biochar	Freundlich	[57]
Other pollutants			
Norfloxacin	Cassava dreg biochar BC 350, pyrolysis at 350 K	Freundlich	[54]
Norfloxacin	Cassava dreg biochar BC 450, pyrolysis at 450 K	Freundlich	[54]
Norfloxacin	Cassava dreg biochar BC 550, pyrolysis at 550 K	Freundlich	[54]
Norfloxacin	Cassava dreg biochar BC 650, pyrolysis at 650 K	Freundlich	[54]
Norfloxacin	Cassava dreg biochar BC 750, pyrolysis at 750 K	Freundlich	[54]
Ciprofloxacin	Cassava dreg biochar (BC350, 550, 750)	Freundlich, Langmuir	[114]

$$q_t = \frac{1}{b}\ln(1 + abt). \quad (35)$$

The nonlinear least squares regression method can be used to solve the nonlinear equation (35) in this example. The nonlinear approach is more difficult than the linear method.

5.5. Ritchie's Equation. The adsorption kinetic data of gases on solids were initially modelled using Ritchie's equation (135). Ritchie's equation's physical significance is that adsorption in active sites dominates all other types of adsorption. Active sites can be occupied by a single adsorbate ion or molecule. In this model, the desorption process is not considered. Ritchie's equation is presented as follows:

$$\frac{d\theta}{dt} = a(1 - \theta)^n. \quad (36)$$

5.6. Pseudo-nth-Order (PNO) Mode. Pb(II) adsorption kinetic data on wheat bran treated with sulphuric acid were modelled by Ozer [136] using pseudo-nth-order (PNO) theory.

$$\mathbf{\frac{dq_t}{dt} = k_n(q_e - q_t)^n}. \quad (37)$$

Table 4 summarizes the kinetic models reported in the literature for adsorption of organic and inorganic contaminants in water and wastewater.

6. Mass Transfer in Adsorption

6.1. External Diffusion Models. The slowest step, according to external diffusion models, is the diffusion of adsorbed species in an enclosing liquid film. To model the intraparticle diffusion process, various equations have been proposed.

6.1.1. Boyd's External Diffusion Equation. Boyd et al. [137] presumed a kinetic expression to designate the diffusion of the adsorbate over a bounding liquid film, as given in equation.

$$\mathbf{\frac{dq_t}{dt} = 4\pi r_o^2 D^1\left(\frac{\partial C_f}{\partial r}\right)_{r=r_o}}. \quad (38)$$

6.1.2. Furusawa–Smith (F–S) Model. Furusawa et al. [138] established an adsorption rate model.

$$\mathbf{\frac{C_t}{C_o} = \frac{1}{1 + m_s K} + \frac{m_s K}{1 + m_s K} e^{-(1+m_s K/m_s K)k_{F\&S}St}}. \quad (39)$$

The value of $k_{F\&S}$ St is used to characterize the exterior diffusional process. The F–S model presupposes that the isotherm is linear, intraparticle diffusion is insignificant, and external diffusion is the slowest step [138]. It should be noted that the adsorption requirement that the isotherm is not linear cannot be modelled by equation (39).

6.1.3. Mathews–Weber (M–W) Model. The Mathews–Weber (M–W) model is offered as follows [139]:

$$\mathbf{k_{M\&W} = \frac{r_O \rho(1 - \varepsilon)}{3m_s} \frac{\ln(C_o/C_t)}{t}}. \quad (40)$$

6.1.4. Phenomenological External Mass Transfer (EMT) Model. According to the EMT model (Equation (41)), equilibrium is reached on the interface of the adsorbent, and film diffusion is assumed to be the slowest process [140]. The gradient in adsorbent concentrations within the liquid film is what drives external diffusion.

$$\mathbf{\frac{dq_t}{dt} = \frac{k_s}{\rho}(C_t - C_{et}) + K_{ext}(C_t - C_{et})}. \quad (41)$$

Then, the adsorption isotherm model describes the equilibrium phenomenon. The isotherm model is presented as $q_{et} = f(C_{et})$. Then, $C_{et} = f^{-1}(q_{et})$.

6.2. Internal Diffusion Models. The slowest step, according to internal diffusion theories, is the diffusion of the adsorbate within the adsorbent. Instantaneous adsorption onto the active sites and adsorbate diffusion in the aqueous film occurs from place to place in the adsorbent. The three most common internal diffusion models, the intraparticle Boyd's diffusion model, Weber and Morris (W–M) model, and phenomenological interior mass transfer (IMT) model, were evaluated in this study.

6.2.1. Boyd's Intraparticle Diffusion Model. Using an intraparticle diffusion model [137], the equation is as follows:

$$\mathbf{F = 1 - \frac{6}{\pi^2}\sum_{n=1}^{\infty}\frac{1}{n^2}e^{-n^2Bt}}. \quad (42)$$

The adsorption equilibrium model yields q (mg·g^1) when $F = q_t/q_\infty$, q_∞ (mg·g^{-1}), and ($q_\infty = f(C_e)$).

6.2.2. Weber–Morris (W–M) Model. A model was developed by Weber and Morris in 1963 to explain the intraparticle diffusion process [141]. The equation presents the W–M model as follows:

$$\mathbf{q_t = k_{W\&M} t^{(1/2)}}. \quad (43)$$

If the intercept is zero, then the governing mechanism is intraparticle diffusion. Otherwise, several processes regulate adsorption.

6.2.3. Phenomenological Internal Mass Transfer (IMT) Model. The simplified form of the IMT model is given as

$$\mathbf{\frac{dq_t}{dt} = k_{int}(q_{et} - q_t)}. \quad (44)$$

Table 4: Kinetic models reported in the literature for adsorption of organic and inorganic contaminants in water and wastewater.

Adsorbate	Adsorbent	Adsorption kinetics	Reference
Metal ions			
Chromium	Cassava peel carbon (CPC)	2^{nd} order (pseudo)	[7]
Cobalt	Cassava peel carbon (CPC)	2^{nd} order (pseudo)	[7]
Chromium	Cassava peel carbon	2^{nd} order (pseudo)	[7]
Cobalt	Cassava peel carbon	2^{nd} order (pseudo)	[7]
Lead	Modified cassava stalk	2^{nd} order (pseudo)	[94]
Zinc	Modified cassava stalk	2^{nd} order (pseudo)	[94]
Nickel	Cassava peel	2^{nd} order (pseudo)	[5]
Cadmium	Modified cassava peel activated by 0.1 mol/L of 36% H_2O_2/98% H_2SO_4/99% NaOH	2^{nd} order (pseudo)	[97]
Lead	Modified cassava peel activated by 0.1 mol/L of 36% H_2O_2/98% H_2SO_4/99% NaOH	2^{nd} order (pseudo)	[97]
Chromium	Modified cassava peel activated by 0.1 mol/L of 36% H_2O_2/98% H_2SO_4/99% NaOH	2^{nd} order (pseudo)	[97]
Lead	Cassava peel carbon	2^{nd} order (pseudo)	[59]
Dyes			
Rhodamine B	Cassava slag biochar	2^{nd} order (pseudo)	[57]
Malachite green	Cassava rind Carbon (CRC)	2^{nd} order (pseudo)	[73]
Methylene blue	Cassava rind Carbon (CRC)	2^{nd} order (pseudo)	[53]
Reactive red + Drimarene turquoise	Cassava stem biochar (CSB)	Pseudofirst-order and Elovich second-order	[61]
Other pollutants			
Norfloxacin	Cassava dreg biochar BC 350, pyrolysis at 350 K	2^{nd} order (pseudo)	[54]
Norfloxacin	Cassava dreg biochar BC 450, pyrolysis at 450 K	2^{nd} order (pseudo)	[54]
Norfloxacin	Cassava dreg biochar BC 550, pyrolysis at 550 K	2^{nd} order (pseudo)	[54]
Norfloxacin	Cassava dreg biochar BC 650, pyrolysis at 650 K	2^{nd} order (pseudo)	[54]
Norfloxacin	Cassava dreg biochar BC 750, pyrolysis at 750 K	2^{nd} order (pseudo)	[54]
Ciprofloxacin	Cassava dreg biochar (BC350, 550, 750)	2^{nd} order (pseudo)	[114]

Table 5: Mass transfer models reported in the literature for adsorption of organic and inorganic contaminants in water and wastewater.

Adsorbate	Adsorbent	Mass transfer/mechanism	Reference
Metal ions			
Nickel	Activated carbon from cassava peel tubers	Solid diffusion	[51]
Nickel	Activated carbon from cassava peel tubers	Solid diffusion	[51]
Nickel	Activated carbon from cassava peel tubers	Solid diffusion	[51]
Nickel	Raw material (RM)	Solid diffusion	[51]
Copper	Modified cassava fibre	Intraparticle diffusion	[86]
Copper	Modified cassava fibre	Intraparticle diffusion	[86]
Chromium	Cassava peel carbon	Solid-liquid diffusion	[7]
Cobalt	Cassava peel carbon	Solid-liquid diffusion	[7]
Cadmium	Untreated cassava peel biomass/acid-treated cassava peel biomass	Diffusion is film diffusion controlled/sorption is particle diffusion controlled	[11]
Zinc	Untreated cassava peel biomass/acid-treated cassava peel biomass	Diffusion is film diffusion controlled/sorption is particle diffusion controlled	[11]
Dyes			
Congo red	Cassava residue	Correlation coefficient <0.95) controlling step distributed between intraparticle and film diffusion	[67]
Other pollutants			
Nitrate	Modified cassava straw	Both surface adsorption and intraparticle diffusion	[64]

Table 6: Evaluation of thermodynamic parameters for adsorption of organic and inorganic contaminants using cassava residues as adsorbents.

Adsorbate	Adsorbent	ΔH (kJ/mol)	ΔS (kJ/mol·K)	ΔG (kJ/mol)	Reference
Metal ions					
Chromium	Cassava peel carbon (CPC)	+18.28	+0.063	−5.58 (288.14 K), −6.29 (298.14 K), and −7.24 (308.14 K)	[7]
Cobalt	Cassava peel carbon (CPC)	+39.64	+0.16	−7.28 (288.14), −8.73 (298.14 K), and −10.45 (308.14 K)	[7]
Lead	Modified cassava stalk	+19.33	+0.148	−24.79 (298.1 K), −26.22 (308.1 K), and −27.75 (318.1 K)	[94]
Zinc	Modified cassava stalk	+34.62	+0.187	−21.24 (298.1 K), −22.72 (308.1 K) and −24.98 (318.1 K)	[94]
Nickel	Cassava peel	+46.584	+0.162	−2.738 (303.15 K), −5.077 (318.15 K), and −7.623 (333.15 K)	[5]
Cadmium	Modified cassava peel activated by 0.1 mol/L of 36% H_2O_2/98% H_2SO_4/99% NaOH	+15.5/5.6/−29.7	43.6/6.5/−0.0852	+3.0, +3.8	[97]
Lead	Modified cassava peel activated by 0.1 mol/L of 36% H_2O_2/98% H_2SO_4/99% NaOH	−59.5/−59.6/−0.26	−0.1942/−0.2039/−0.0755	+3.8	[97]
Chromium	Modified cassava peel activated by 0.1 mol/L of 36% H_2O_2/98% H_2SO_4/99% NaOH	−5.7/−9.9/+18.1	−0.0151/−0.034/+0.074	—	[97]
Lead	Grafted cassava starch	−7.6971511	−0.0079078	−5.327971 (298 K), −5.2810872 (308 K), and −5.1681819 (318 K)	[113]
Lead	Cassava peel carbon	+12.762	+0.0672	−7.67492 (303 K), −8.16296 (313 K), −8.80059 (323 K), and −9.71912 (333 K)	[59]
Dyes					
Methylene blue	Cassava rind carbon (CRC)	+17.4	+0.074	−4.86 (298.15 K), −5.02 (303.14 K), −5.47 (308.14 K), −6.00 (313.14 K), and −6.24 (318.14 K)	[53]
Malachite green	Cassava rind carbon (CRC)	+20–80	+0.23	−8.791 (293.14 K), −12.775 (308.14 K), and −14.947 (323.14 K)	[73]
Reactive red + Drimarene turquoise	Cassava stem biochar (CSB)	−15.92	−66.13	—	[61]
Crystal violet	Raw cassava peel powder	−20.536	−46.484	−6.65(303.1 K), −6.01 (313.1 K), −5.18 (325.1 K), −4.93 (333.01 K), and − 4.76 (343.1 K)	[63]
Rhodamine B	Cassava slag biochar	+0.2225	+0.001192	−8.116 (308 K), −8.478 (318 K), and −9.196 (328 K)	[57]

Table 6: Continued.

Adsorbate	Adsorbent	ΔH (kJ/mol)	ΔS (kJ/mol·K)	ΔG (kJ/mol)	Reference
Other pollutants					
Norfloxacin	Cassava dreg biochar BC 350, pyrolysis at 350 K	−34.14	−0.10	−6.29 (288.1 K), −5.54 (298.1 K), and −4.36 (308.1 K)	[54]
Norfloxacin	Cassava dreg biochar BC 450, pyrolysis at 450 K	+1.45	+0.05	−13.24 (288.1 K), −13.98 (298.1 K), and −14.27 (308.1 K)	[54]
Norfloxacin	Cassava dreg biochar BC 550, pyrolysis at 550 K	+47.45	+0.21	−11.85 (288 K), −14.37 (298 K), and −15.98 (308 K)	[54]
Norfloxacin	Cassava dreg biochar BC 650, pyrolysis at 650 K	+331.41	+1.31	−47.59 (288 K), −58.34 (298 K), and −73.85(308 K)	[54]
Norfloxacin	Cassava dreg biochar BC 750, pyrolysis at 750 K	+326.40	+1.32	−52.28 (288 K), −66.12 (298 K), and −78.60 (308 K)	[54]
Ciprofloxacin	Cassava dreg biochar (BC350/550/750)	−48.93 (350 K), −15.23 (550 K), and −83.62 (750 K)	−0.13 (350 K), −1.19 (550 K), and −0.25 (750 K)	−11.63 (350 K), −14.29 (550 K), and −13.03 (750 K)	[114]

6.3. Pore Volume and the Surface Diffusion (PVSD) Model. The PVSD model's fundamental presumptions are as follows: the adsorbent particle is globular, the solution is homogeneous, the convective mass transfer in pores is low, and the adsorption of substances on active sites is simultaneous. The equation describes the PVSD model [142].

$$\mathbf{V}\frac{\mathbf{dC_t}}{\mathbf{dt}} = -\mathbf{mS_p k_F}\left(\mathbf{C_t} - \mathbf{C_{tr@r=r_0}}\right). \tag{45}$$

Table 5 summarizes the mass transfer models reported in the literature for adsorption of organic and inorganic contaminants in water and wastewater.

7. Adsorption Thermodynamics

The Van't Hoff equation is used to explain the thermodynamics in adsorption systems [143]. The equation is as follows:

$$\ln \mathbf{K_e} = -\frac{\Delta \mathbf{H^o}}{\mathbf{RT}} + \frac{\Delta \mathbf{S^o}}{\mathbf{R}}. \tag{46}$$

Table 6 shows the thermodynamic values for standard enthalpy, entropy, and Gibbs free energy of adsorption for various cassava-based adsorbents.

8. Challenges and Future Prospectives

Cassava has drawbacks of quick deterioration, lack of active sites, and lesser surface areas when it is used in raw powder. Also, presence of toxins in cassava limits its applications for food and feed. Hence, cassava requires carbonisation and activation to utilize it as an adsorbent with improved thermal stability, abundance of active sites, and enhanced surface areas.

9. Conclusion

The present review focussed on parameters affecting adsorption, preparation, and activation methods of cassava-based adsorbents, adsorption isotherms, kinetics, thermodynamics, and binding mechanisms through mass transfer studies. As cassava contains active functional groups, has better electron transfer, and has smaller particle size, cassava stem, rhizome, peel, and bagasse could be potential materials for adsorbents for removal of organic and inorganic pollutants from water and wastewater.

Data Availability

The authors confirm that the data supporting the findings of this study are available within the article.

Conflicts of Interest

The authors declare that they have no conflicts of interest.

Acknowledgments

The authors would like to express their deep gratitude to the management of the Sathyabama Institute of Science and Technology, India, and the University of Technology and Applied Sciences, Oman, for their support to carry out the present work.

References

[1] O. A. Otekunrin and B. Sawicka, "Cassava, a 21st century staple crop: how can Nigeria harness its enormous trade potentials," *Acta Scientific Agriculture*, vol. 3, no. 8, pp. 194–202, 2019.

[2] A. A Fathima, M Sanitha, L. Tripathi, S. Muiruri, L. Tripathi, and S. Muiruri, "Cassava (Manihot esculenta) dual use for food and bioenergy: Cassava (*Manihot esculenta*) dual use for food and bioenergy," *Food and Energy Security*, vol. 12, p. 380, 2022.

[3] F. S. Dinata and I. S. Kartawiria, "Bioethanol potential from whole parts of cassava plant in Indonesia," *Jurnal Teknologi Industri Pertanian*, vol. 31, no. 1, pp. 20–33, 2021.

[4] Fao, "Food agricultural organization statistics," 2019, https://knoema.com/atlas/sources/FAO.

[5] A. Kurniawan, A. N. Kosasih, J Febrianto et al., "Evaluation of cassava peel waste as lowcost biosorbent for Ni-sorption: Evaluation of cassava peel waste as lowcost biosorbent for Ni-sorption: Equilibrium, kinetics, thermodynamics and mechanismquilibrium, kinetics, thermodynamics and mechanism," *Chemical Engineering Journal*, vol. 172, no. 1, pp. 158–166, 2011.

[6] K. Philip, R. Jacob, and J. Gopalakrishnan, "Characterization of Characterization of Cassava Root Husk Powder: Equilibrium, Kinetic and Modeling Studies as Bioadsorbent for Copper(II) and Lead(II)assava root husk powder: equilibrium, kinetic and modeling studies as bioadsorbent for copper (II) and lead (II)," *Journal of Encapsulation and Adsorption Sciences*, vol. 11, no. 02, pp. 69–86, 2021.

[7] A. Belcaid, B. H Beakou, K. El Hassani, A. Anouar, S. Bouhsina, and A. Anouar, "Efficient removal of Cr (VI) and Co (II) from aqueous solution by activated carbon from Manihot esculenta Crantz agricultural bio-waste," *Water Science and Technology*, vol. 83, no. 3, pp. 556–566, 2021.

[8] C. Parvathi, T. Maruthavanan, S. Sivamani, and C. Prakash, "Biosorption studies for the removal of malachite green from its aqueous solution by activated carbon prepared from cassava peel," *E-Journal of Chemistry*, vol. 8, no. 1, pp. S61–S66, 2011.

[9] I. S. Bădescu, D Bulgariu, I. Ahmad, L. Bulgariu, I. Ahmad, and L. Bulgariu, "Valorisation possibilities of exhausted biosorbents loaded with metal ions – Valorisation possibilities of exhausted biosorbents loaded with metal ions – A review review," *Journal of Environmental Management*, vol. 224, pp. 288–297, 2018.

[10] J. Fonseca, A. Albis, A. Montenegro, and R. R. Montenegro, "Evaluation of zinc adsorption using cassava peels (Manihot esculenta) modified with citric acid," *Contemporary Engineering Sciences*, vol. 11, no. 72, pp. 3575–3585, 2018.

[11] M. Horsfall and A. A. Abia, "Sorption of cadmium (II) and zinc (II) ions from aqueous solutions by cassava waste biomass (Manihot sculenta Cranz)," *Water Research*, vol. 37, no. 20, pp. 4913–4923, 2003.

[12] O. Ijaola, O. Omotosho, and A. Sangodoyin, "Comparison of heavy metal adsorption form carbons activated with zinc chloride salt (A case study of cassava and bamboo biomass)," 2012, https://www.researchgate.net/profile/Ijaola-Opololaoluwa/publication/348280634_PosterPresentations_for_ICWRE_2014_by_Ijaola_and_Omotosho/links/5ff620084585155

3a0262671/PosterPresentations-for-ICWRE-2014-by-Ijaola-and-Omotosho.pdf.

[13] S. Daniel, C. G Affonso, C. Juliana, P. Ad iacute lson, G. P. Ivone, and F. C. Gustavo, "Removal of Cr (III) from contaminated water using industrial waste of the cassava as natural adsorbents," *African Journal of Agricultural Research*, vol. 10, no. 46, pp. 4241–4251, 2015.

[14] K. N. Awokoya, O. J. Owoade, B. A. Moronkola et al., "Morphological characteristics of cassava peel and its effect on the adsorption of heavy metal ions from aqueous media," *Journal of Multidisciplinary Engineering Science and Technology*, vol. 3, no. 8, pp. 5342–5348, 2016.

[15] M. J. Horsfall, A. I. Spiff, and A. A. Abia, "Studies on the influence of mercaptoacetic acid (MAA) modification of cassava (Manihot sculenta Cranz) waste biomass on the adsorption of Cu 2+ and Cd 2+ from aqueous solution," *Bulletin of the Korean Chemical Society*, vol. 25, no. 7, pp. 969–976, 2004.

[16] S. Ismadji, . *Utilization of Agricultural Waste Biomass for Treatment of Wastewater Containing Heavy Metal*, Academia.Edu, San Francisco, CA, USA, 2009.

[17] Y. Ja'afar and A. O. Lawal, "Studies on interference of adsorption of heavy metal ions on chelating sorbents from cassava and Amidoxime-modified Polyacrylonitrile-grafted-Cassava Starch," *Nigerian Journal of Chemical Research*, vol. 22, no. 2, pp. 54–60, 2017.

[18] A. Jorgetto, R Silva, M. Saeki et al., "Cassava root husks powder as green adsorbent for the removal of Cu (II) from natural river water," *Applied Surface Science*, vol. 288, pp. 356–362, 2014.

[19] E. C. Junior, D. Schwantes, A. C. Gonçalves, and A. G. Rosenberger, "Modified cassava barks as an adsorbent of copper ions," in *Book of Proceedings 5th International Conference on Sustainable Development*p. 23, European Center of Sustainable Development Cesare Anselmi, Rome Italy, 2017.

[20] H. Owamah, "Sorption kinetic models of Pb (II) and Cu (II) from a typical hospital wastewater using modified cassava peels (MCP) biomass," *Journal of International Environmental Application & Science*, vol. 7, no. 4, pp. 721–733, 2012.

[21] H. I. Owamah and I. Owamah, "Biosorptive removal of Pb(II) and Cu(II) from wastewater using activated carbon from cassava peels," *Journal of Material Cycles and Waste Management*, vol. 16, no. 2, pp. 347–358, 2014.

[22] J. Luo, C. Ge, H. Yu, D. Fenk, P. Huang, and F. Li, "Cassava waste derived biochar as soil amendments: effects on Kinetics, equilibrium and thermodynamic of atrazine adsorption," *Fresenius Environmental Bulletin*, vol. 25, pp. 4607–4617, 2016.

[23] T. Mutiara, F. I. Muhandi, A. Alhumaini, A. Chafidz, and H. Pratikno, "Removal of lead (Pb^{2+}) from aqueous solution using bio-adsorbent prepared from cassava stem pith," in *Materials Science Forum*, vol. 981, pp. 331–335, Trans Tech Publications Ltd, Wollerau, Switzerland, 2020.

[24] J. Shi, H. Luo, D. Xiao et al., "Bio-sorbents from cassava waste biomass and its performance in removal of Pb^{2+} from aqueous solution," *Journal of Applied Polymer Science*, vol. 131, no. 2, 2014.

[25] N. Supamathanon, N. Butwong, K. Jansungnean, and P. Voanok, "Modification of cassava residue for the adsorption of Pb (II) ion from aqueous solution," *Burapha Science Journal*, vol. 22, no. 2, pp. 274–287, 2017.

[26] A. Suprabawati, N. W. Holiyah, J. Jasmansyah, U. Jenderal Achmad Yani, and J. Terusan Jenderal Sudirman, "Activated Kulit Singkong (Manihot esculenta Crantz) sebagai Karbon Aktif Dengan berbagai langkah pembuatan untuk Adsorpsi Logam Timbal (Pb2+) dalam airarbon from cassava peel as adsorbent of lead metal (Pb2+) in the water," *Jurnal Kartika Kimia*, vol. 1, 2018.

[27] C. Tejada-Tovar, A. Villabona-Ortíz, and A. D. González-Delgado, *Agricultural Residues of cocoa, Lemon, Yam, Cassava and Oil palm for lead-loaded Wastewater Treatment*, Universidad Santiago de cali, Valle del Cauca, Colombia, 2000.

[28] A. Villabona-Ortíz, C. Tejada-Tovar, and A. Gonzalez-Delgado, "Application of cement-based solidification/stabilization technique for immobilizing lead and nickel ions after sorption-desorption cycles using cassava peels biomass," *Indian Journal of Science and Technology*, vol. 11, no. 45, pp. 1–4, 2017.

[29] E. A. Pondja Jr, K M Persson, N. P. Matsinhe, K. M. Persson, and N. P. Matsinhe, "The potential use of cassava peel for treatment of mine water in Mozambique," *Journal of Environmental Protection*, vol. 08, no. 3, pp. 277–289, 2017.

[30] S. Ndlovu, G. S. Simate, L. Seepe, A. Shemi, V. Sibanda, and L. D. Van Dyk, "The removal of Co^{2+}, V^{3+} and Cr^{3+} from waste effluents using cassava waste," *South African Journal of Chemical Engineering*, vol. 18, no. 1, pp. 51–69, 2013.

[31] M. Vasudevan, P. Ajithkumar, R Singh, N. Natarajan, R. P. Singh, and N. Natarajan, "Mass transfer kinetics using two-site interface model for removal of Cr (VI) from aqueous solution with cassava peel and rubber tree bark as adsorbents," *Environmental Engineering Research*, vol. 21, no. 2, pp. 152–163, 2016.

[32] A. D. O. Jorgetto, A. C. P. D. Silva, B. Cavecci, R. C. Barbosa, M. A. U. Martines, and G. R. D. Castro, "Cassava root husks as a sorbent material for the uptake and pre-concentration of cadmium (II) from aqueous media," *Orbital - The Electronic Journal of Chemistry*, vol. 5, pp. 206–212, 2013.

[33] Z. Luo, S. Luo, C. Niu, S. Hu, L. Chen, and C. Fan, "Removal of Pb^{2+} and Cd^{2+} from aqueous solutions by chemically modified cellulose of cassava waste," *Fresenius Environmental Bulletin*, vol. 25, p. 5326, 2016.

[34] E. Ofudje, E. Sodiya, F. Ibadin, A. Ogundiran, O. Osideko, and A. Uzosike, "Sorption of Cd^{2+} from aqueous solutions using cassava (manihot esculenta) waste: equilibrium and kinetic studies," *Journal of Chemical Society of Nigeria*, vol. 45, no. 3, 2020.

[35] K. Kadirvelu, C. Karthika, N. Vennilamani, and S. Pattabhi, "Activated carbon from industrial solid waste as an adsorbent for the removal of Rhodamine-B from aqueous solution: Activated carbon from industrial solid waste as an adsorbent for the removal of Rhodamine-B from aqueous solution: Kinetic and equilibrium studiesinetic and equilibrium studies," *Chemosphere*, vol. 60, no. 8, pp. 1009–1017, 2005.

[36] P. Ndagijimana, X. Liu, Q. Xu et al., "Cassava flour extracts solution to induce gelatin cross-linked activated carbon-graphene oxide composites: Cassava flour extracts solution to induce gelatin cross-linked activated carbon-graphene oxide composites: The adsorption performance of dyes from aqueous mediahe adsorption performance of dyes from aqueous media," *Environmental Advances*, vol. 5, Article ID 100079, 2021.

[37] K. Junlapong, P. Maijan, C. Chaibundit, and S. Chantarak, "Effective adsorption of methylene blue by biodegradable superabsorbent cassava starch-based hydrogel," *International Journal of Biological Macromolecules*, vol. 158, pp. 258–264, 2020.

[38] Y. Lisafitri, "Preliminary studies of cassava leaves' ability to remove dyes from water," *Journal of Mathematical & Fundamental Sciences*, vol. 52, no. 1, 2020.

[39] L. Meili, R. P. S Godoy, J I Soletti et al., "Cassava (Manihot esculenta Crantz) stump biochar: Cassava (*Manihot esculenta* Crantz) stump biochar: Physical/chemical characteristics and dye affinityhysical/chemical characteristics and dye affinity," *Chemical Engineering Communications*, vol. 206, no. 7, pp. 829–841, 2019.

[40] D. Soto, O. León, A. Muñoz-Bonilla, and M. Fernandez-García, "Succinylated starches for dye removal," *Starch - Stärke*, vol. 73, no. 2, Article ID 2000043, 2021.

[41] C. Parvathi, U. S. Shoba, C. Prakash, and S. Sivamani, "Manihot esculenta peel powder: effective adsorbent for removal of various textile dyes from aqueous solutions," *Journal of Testing and Evaluation*, vol. 46, no. 6, Article ID 20170160, 2018.

[42] P. Huang, C. Ge, D. Feng et al., "Effects of metal ions and pH on ofloxacin sorption to cassava residue-derived biochar," *Science of the Total Environment*, vol. 617, pp. 1384–1391, 2018.

[43] J. Luo, X. Li, C. Ge et al., "Preparation of ammonium-modified cassava waste-derived biochar and its evaluation for synergistic adsorption of ternary antibiotics from aqueous solution," *Journal of Environmental Management*, vol. 298, Article ID 113530, 2021.

[44] R. Rinawati, S. Supriyanto, and Y. O. Kasih, "Preparation of magnetic activated carbon from cassava peel for removal of tetracycline antibiotic in aquatic environment," 2020, http://repository.lppm.unila.ac.id/25713/1/Abstract%20icasmi%202020.pdf.

[45] C. Netoa, W. Costab, Y. Diasc, and M. Santosa, *Phosphorus Adsorption in Aqueous Medium Using Biocarbon from Cassava Agricultural Residue (Manihot Esculenta)*, Universidade Federal do Ceará, Fortaleza, Brazil, 2021.

[46] M. G. Gomes, D Q Santos, L. C. d. Morais et al., "Purification of biodiesel by dry washing and the use of starch and cellulose as natural adsorbents: Part II–study of purification times," *Biofuels*, vol. 12, no. 5, pp. 579–587, 2021.

[47] I. Ilaboya, R. Ilaboya, E. O. Oti, G. O. Ekoh, and L. O. Umukoro, "Performance of Activated Carbon from Cassava Peels for the Treatment of Effluent Wastewater," *Iranica Journal of Energy and Environment*, vol. 4, no. 4, 2013.

[48] O. A. Omotosho, A Y Sangodoyin, A. Omotosho, and A. Y. Sangodoyin, "Production and utilization of cassava peel activated carbon in treatment of effluent from cassava processing industry," *Water Practice and Technology*, vol. 8, no. 2, pp. 215–224, 2013.

[49] D. F Simatupang, JF. Tarigan, Simatupang, and J. Tarigan, "The effect of active carbon adsorbents from some wastes in reducing free fatty acids and acid number to improve vco quality," *IOP Conference Series: Materials Science and Engineering*, vol. 885, no. 1, Article ID 12011, 2020.

[50] J. d. O. Primo, C. Bittencourt, S. Acosta et al., "Synthesis of Synthesis of Zinc Oxide Nanoparticles by Ecofriendly Routes: Adsorbent for Copper Removal From Wastewaterinc oxide nanoparticles by ecofriendly routes: adsorbent for copper removal from wastewater," *Frontiers in Chemistry*, vol. 8, Article ID 571790, 2020.

[51] B. A. A. Alongamo, L D Ajifack, J. N. Ghogomu et al., "Activated Activated Carbon from the Peelings of Cassava Tubers (Manihot esculenta) for the Removal of Nickel(II) Ions from Aqueous Solutionarbon from the peelings of cassava tubers (manihot esculenta) for the removal of nickel (II) ions from aqueous solution," *Journal of Chemistry*, vol. 2021, Article ID 5545110, 14 pages, 2021.

[52] M. A Abia, S. Ai, A. A. Arbia, and A. I. Spiff, "Removal of Cu (II) and Zn (II) ions from wastewater by cassava (Manihot esculenta Cranz) waste biomass," *African Journal of Biotechnology*, vol. 2, no. 10, pp. 360–364, 2003.

[53] B. H. Beakou, K. El Hassani, M. A. Houssaini et al., "Novel activated carbon from Novel activated carbon from Manihot esculenta Crantz for removal of Methylene Blueanihot esculenta crantz for removal of methylene blue," *Sustainable Environment Research*, vol. 27, no. 5, pp. 215–222, 2017.

[54] D. Feng, H. Yu, H. Deng, F. Li, and C. Ge, "Adsorption characteristics of norfloxacin by biochar prepared by cassava dreg: kinetics, isotherms, and thermodynamic analysis," *Bioresources*, vol. 10, no. 4, pp. 6751–6768, 2015.

[55] E. A. Abia, O. B. Didi, and E. D. Asuquo, "Modeling of Cd" Modeling of Cd2+ Sorption Kinetics from Aqueous Solutions onto Some Thiolated Agricultural Waste Adsorbent-sorption kinetics from aqueous solutions onto some thiolated agricultural VVaste adsorbents," *Journal of Applied Sciences*, vol. 6, no. 12, pp. 2549–2556, 2006.

[56] M. Gunasegaran, "Removal of metanil yellow dye from aqueous solution using cassava peel," Doctoral dissertation, Universiti Malaysia Kelantan, Kota Bharu, Malaysia, 2019.

[57] J. Wu, J. Yang, G. Huang, C. Xu, and B. Lin, "Hydrothermal carbonization synthesis of cassava slag biochar with excellent adsorption performance for Rhodamine B," *Journal of Cleaner Production*, vol. 251, Article ID 119717, 2020.

[58] N. S. Hassan, "Cassava peel as adsorbent for removal of malachite green dye," Doctoral dissertation, Universiti Malaysia Kelantan, Kota Bharu, Malaysia, 2018.

[59] C. O. Thompson, A O Ndukwe, C. O. Asadu, A. O. Ndukwe, and C. O. Asadu, "Application of activated biomass waste as an adsorbent for the removal of lead (II) ion from wastewater," *Emerging Contaminants*, vol. 6, pp. 259–267, 2020.

[60] Y. Ja'afar, S. A. M. Jamil, A. O. Lawal, B. Y. Jamoh, and A. Muhammad, "Removal of Cu (II) by amidoxime-modified polyacrylonitrile-grafted-cassava starch," *Nigerian Journal of Chemical Research*, vol. 21, pp. 33–50, 2016.

[61] A. Navya, S. Nandhini, S. Sivamani et al., "Preparation and characterization of cassava stem biochar for mixed reactive dyes removal from simulated effluent," *Desalination and Water Treatment*, vol. 189, pp. 440–451, 2020.

[62] L. N. Dos Santos, C E Porto, M. K. Bulla et al., "Peach palm and cassava wastes as biosorbents of tartrazine yellow dye and their application in industrial effluent," *Scientia Plena*, vol. 17, no. 5, 2021.

[63] N. J. Okorocha, C. K. Enenebeaku, M. O. Chijioke-Okere, C. E. Ohaegbulam, and C. E. Ogukwe, "Adsorptive removal of crystal violet using agricultural waste: equilibrium, kinetic and thermodynamic studies," *American Journal of Engineering Research*, vol. 8, 2019.

[64] W. Li, W. Mo, M. Zhang, M. Meng, and M. Chen, "Adsorption of nitrate from aqueous solution onto modified cassava (Manihot esculenta) straw/Adsorpcja azotanow z roztworu wodnego na zmodyfikowanej slomie manioku Manihot esculenta," *Ecological Chemistry and Engineering S*, vol. 19, no. 4, pp. 629–638, 2012.

[65] M. L. Theng and L. S. Tan, "Optimization on methylene blue and Congo red dye adsorption onto cassava leaf using response surface methodology," *Malaysian Journal of Catalysis*, vol. 4, no. 2, 2020.

[66] F. B Scheufele, J Staudt, M. H. Ueda et al., "Biosorption of direct black dye by cassava root husks: Biosorption of direct black dye by cassava root husks: Kinetics, equilibrium, thermodynamics and mechanism assessmentinetics, equilibrium, thermodynamics and mechanism assessment," *Journal of Environmental Chemical Engineering*, vol. 8, no. 2, Article ID 103533, 2020.

[67] H. X Li, R J Zhang, L. Tang et al., "Use of cassava residue for the removal of Congo red from aqueous solution by a novel process incorporating adsorption and in vivo decolorization," *BioResources*, vol. 9, no. 4, pp. 6682–6698, 2014.

[68] C. Tejada-Tovar, A. Villabona-Ortz, A. Herrera-Barros et al., "Adsorption kinetics of Cr (VI) using modified residual biomass in batch and continuous system," *Indian Journal of Science and Technology*, vol. 11, no. 14, pp. 1–8, 2018.

[69] F. Sulaiman, M. Septiani, S. Aliyasih, and N. Huda, "Effectiveness of a cassava peel adsorbent on the absorption of copper (Cu2+) and zinc (Zn2+) metal ions," *International Journal on Advanced Science, Engineering and Information Technology*, vol. 9, no. 4, pp. 1296–1301, 2019.

[70] A. J. Rubio, I. Z. Da Silva, F. Gasparotto et al., "Removal of methylene blue using cassava bark residue," *Chemical Engineering Transactions*, vol. 65, pp. 751–756, 2018.

[71] S. D. Aulia, A Wijayanti, R. Hadisoebroto, A. Wijayanti, and R. Hadisoebroto, "The effect of mixing speed and contact time on dye removal using Cassava Peel adsorbents," *IOP Conference Series: Earth and Environmental Science*, vol. 737, no. 1, Article ID 12013, April, 2021.

[72] C. Tejada Tovar, A. Villabona Ortiz, and L. E. Garcés Jaraba, "Kinetics of adsorption in mercury removal using cassava (Manhiot esculenta) and lemon (Citrus limonum) wastes modified with citric acid," *Ingeniería Y Universidad*, vol. 19, no. 2, pp. 283–298, 2015.

[73] B. H. Beakou, K. El Hassani, M. A. Houssaini, M. Belbahloul, E. Oukani, and A. Anouar, "A novel biochar from Manihot esculenta Crantz waste: application for the removal of Malachite Green from wastewater and optimization of the adsorption process," *Water Science and Technology*, vol. 76, no. 6, pp. 1447–1456, 2017.

[74] A. R. Lucaci, D Bulgariu, I. Ahmad et al., "Potential use of biochar from various waste biomass as biosorbent in Co (II) removal processes," *Water*, vol. 11, no. 8, p. 1565, 2019.

[75] S. Y. Foong, N S Abdul Latiff, R. K. Liew et al., "Production of biochar for potential catalytic and energy applications via microwave vacuum pyrolysis conversion of cassava stem," *Materials Science for Energy Technologies*, vol. 3, pp. 728–733, 2020.

[76] A. H. Omar, K Ramesh, A. M. A. Gomaa, B. M. Y. Rosli, A. M. A. Gomaa, and M. Y. Rosli, "Experimental design technique on removal of hydrogen sulfide using CaO-eggshells dispersed onto palm kernel shell activated carbon: Experimental design technique on removal of hydrogen sulfide using CaO-eggshells dispersed onto palm kernel shell activated carbon: Experiment, optimization, equilibrium and kinetic studiesxperiment, optimization, equilibrium and kinetic studies," *J. Wuhan Univ. Technol. Mater. Sci. Ed.*vol. 32, no. 2, pp. 305–320, 2017.

[77] O. A. Habeeb, K Ramesh, G. A. Ali, R. B. M. Yunus, G. A. Ali, and B. Rosli, "Low-cost and eco-friendly activated carbon from modified palm kernel shell for hydrogen sulfide removal from wastewater: Low-cost and eco-friendly activated carbon from modified palm kernel shell for hydrogen sulfide removal from wastewater: adsorption and kinetic studiesdsorption and kinetic studies," *Desalination and Water Treatment*, vol. 84, pp. 205–214, 2017.

[78] G. A. M. Ali, O A Habeeb, H. Algarni et al., "CaO impregnated highly porous honeycomb activated carbon from agriculture waste: symmetrical supercapacitor study," *Journal of Journal of Materials Scienceaterials Science*, vol. 54, no. 1, pp. 683–692, 2019.

[79] G. A. Ali, S A. Manaf, K. F Chong et al., "Superior supercapacitive performance in porous nanocarbons," *Journal of Journal of Energy Chemistrynergy Chemistry*, vol. 25, no. 4, pp. 734–739, 2016.

[80] G. A. Ali, M. M. Yusoff, and K. F. Chong, "Graphene: electrochemical production and its energy storage properties," *ARPN J Eng Appl Sci*, vol. 11, no. 16, pp. 9712–9717, 2016.

[81] G. Hegde, S. A. Abdul Manaf, A Kumar et al., "Biowaste sago bark based catalyst free carbon nanospheres: waste to wealth approach," *ACS Sustainable Chemistry & Engineering*, vol. 3, no. 9, pp. 2247–2253, 2015.

[82] N. Tri Widayati, T. Darsono, S. Negeri, J. Kiai Cebolang, and M. Pati, "Effectiveness of activated carbon from cassava peel waste to reduce TSS (total solid suspended) levels in batik liquid waste," in *Proceedings of the 5th International Conference on Science, Education and Technology, ISET 2019*, Central Java, Indonesia, June 2020.

[83] G. K Ndongo, N J Nsami, K. J. Mbadcam, N. J. Nsami, and K. J. Mbadcam, "Ferromagnetic activated carbon from cassava (Manihot dulcis) peels activated by Iron (III) chloride: Ferromagnetic activated carbon from cassava (Manihot dulcis) peels activated by iron(III) chloride: Synthesis and characterizationynthesis and characterization," *BioResources*, vol. 15, no. 2, pp. 2133–2146, 2020.

[84] C. V. Abiaziem, A. B. Williams, A. Ibijoke Inegbenebor, C. T. Onwordi, C. Osereme Ehi-Eromosele, and L. F. Petrik, "Adsorption of lead ion from aqueous solution unto cellulose nanocrystal from cassava peel," *Iopscience.Iop.Org.*vol. 12122, 2019.

[85] G. O. Agiri and O. Akaranta, "Adsorption of metal ions by dye treated cassava mesocarp," *Scientific Research and Essay*, vol. 4, no. 5, pp. 526–530, 2009.

[86] A. A. Augustine, B. D. Orike, and A. D. Edidiong, "Adsorption kinetics and modeling of Cu (II) ion sorption from aqueous solution by mercaptoacetic acid modified cassava (manihot sculenta cranz) wastes," *EJEAFChe*, vol. 6, no. 4, pp. 2221–2234, 2007.

[87] W. Bai, L. Fan, Y. Zhou et al., "Removal of Cd^{2+} ions from aqueous solution using cassava starch–based superabsorbent polymers," *Journal of Applied Polymer Science*, vol. 134, no. 17, 2017.

[88] I. Candrawati, F. Martak, and Y. I. Cahyo, "Absorption activity of cassava peel (manihot utilissima) as chromium (VI) metal biosorbent in electroplating waste," *The Journal of Pure and Applied Chemistry Research*, vol. 6, no. 2, p. 117, 2017.

[89] H. O. Chukwuemeka-Okorie, F. K. Ekuma, K. G. Akpomie, J. C. Nnaji, and A. G. Okereafor, "Adsorption of tartrazine and sunset yellow anionic dyes onto activated carbon derived from cassava sievate biomass," *Applied Water Science*, vol. 11, 2021.

[90] W. A. Gin, A. Jimoh, A. S. Abdulkareem, and A. Giwa, "Kinetics and isotherm studies of heavy metal removals from electroplating wastewater using cassava peel activated carbon," *Adsorption*, vol. 1000, p. 1, 2014.

[91] X. Guo, C. Chen, and J. Wang, "Sorption of sulfamethoxazole onto six types of microplastics," *Chemosphere*, vol. 228, pp. 300–308, 2019.

[92] A. Herrera-Barros, C. Tejada-Tovar, A. Villabona-Ortiz, A. Gonzalez-Delgado, and L. Fornaris-Lozada, "Effect of pH and particle size for lead and nickel uptake from aqueous solution using cassava (Manihot esculenta) and yam (Dioscorea alata) residual," *Indian Journal of Science and Technology*, vol. 11, 2018.

[93] M. Horsfall, A. A. Abia, and A. I. Spiff, "Kinetic studies on the adsorption of Cd^{2+}, Cu^{2+} and Zn^{2+} ions from aqueous solutions by cassava (Manihot sculenta Cranz) tuber bark waste," *Bioresource Technology*, vol. 97, no. 2, pp. 283–291, 2006.

[94] C. Kang, Q. Li, H. Yi et al., "EDTAD-modified cassava stalks loaded with Fe_3O_4: highly efficient removal of Pb^{2+} and Zn^{2+} from aqueous solution," *Environ. Sci. Pollut. Res.*vol. 28, pp. 6733–6745, 2021.

[95] K. M. Oghenejoboh, S. O. Otuagoma, and E. O. Ohimor, "Application of cassava peels activated carbon in the treatment of oil refinery wastewater–a comparative analysis," *Journal of Ecological Engineering*, vol. 17, no. 2, 2016.

[96] S. Prapagdee, S. Piyatiratitivorakul, and A. Petsom, "Activation of cassava stem biochar by physico-chemical method for stimulating cadmium removal efficiency from aqueous solution," *EnvironmentAsia*, vol. 7, no. 2, 2014.

[97] D. Schwantes, A. C. Gonçalves, G. F. Coelho et al., "Chemical modifications of cassava peel as adsorbent material for metals ions from wastewater," *Journal of Chemistry*, vol. 2016, Article ID 3694174, 15 pages, 2016.

[98] P. U. Shah, N. P. Raval, and N. K. Shah, "Adsorption of copper from an aqueous solution by chemically modified cassava starch," *J Mater Environ Sci*, vol. 6, no. 9, pp. 2573–2582, 2015.

[99] P. T. Tho, H. T. Van, L. H. Nguyen et al., "Enhanced simultaneous adsorption of as (iii), Cd (ii), Pb (ii) and Cr (vi) ions from aqueous solution using cassava root husk-derived biochar loaded with ZnO nanoparticles," *RSC Advances*, vol. 11, no. 31, Article ID 18881, 2021.

[100] A. A. Albis, A. J. López and M. C. Romero, Removal of methylene blue from aqueous solutions using cassava peel (Manihot esculenta) modified with phosphoric acid," *Prospectiva*, vol. 15, no. 2, pp. 60–73, 2017.

[101] A. K. Anas, A. Izzah, S. Y. Pratama, and F. I. Fajarwati, "Removal of methylene blue using biochar from cassava peel (Manihot utilissima) modified by sodium dodecyl sulphate (SDS) surfactant," *AIP Conference Proceedings*, vol. 2229, 2020.

[102] S. Sivakumar, P. Senthilkumar, and V. Subburam, "Carbon from cassava peel, an agricultural waste, as an adsorbent in the removal of dyes and metal ions from aqueous solution," *Bioresource Technology*, vol. 80, no. 3, pp. 233–235, 2001.

[103] W. Astuti, M. Hidayah, L. Fitriana, M. A. Mahardhika, and E. F. Irchamsyah, "Preparation of activated carbon from cassava peel by microwave-induced H3PO4 activation for naphtho$_l$ b$_l$ue-black removal," *AIP Conference Proceedings*, vol. 2243, Article ID 20003, 2020.

[104] M. L. Theng, L. S. Tan, and W. C. Siaw, "Adsorption of methylene blue and Congo red dye from water onto cassava leaf powder," *Progress in Energy and Environment*, vol. 12, pp. 11–21, 2020.

[105] S. Mutiaradini, L. Efiyanti, G. Pari, and B. M. Soebrata, "The utilization of activated carbon from cassava stems on the glucose and cholesterol adsorption," *IOP Conference Series: Materials Science and Engineering*, vol. 980, no. 1, Article ID 12028, 2020.

[106] O. Omotosho, "Mitigation of nitrate pollution in wastewater: a case study of the treatment of cassava processing effluent using cassava peel carbon material," *International Journal of Environmental, Chemical, Ecological, Geological and Geophysical Engineering*, vol. 9, pp. 399–404, 2016.

[107] N. Salahudeen, S. Nakakana, N. Salahudeen, C. S. Ajinomoh, and S. Nakakana, "Adsorption isotherm study for activated carbon produced from cassava peel," *Researchgate.Net.*vol. 4, pp. 8–12, 2014.

[108] N. Ayawei, A. N. Ebelegi, D Wankasi, N. Ebelegi, and D. Wankasi, "Modelling and interpretation of adsorption isotherms," *Journal of Chemistry*, vol. 2017, Article ID 3039817, 11 pages, 2017.

[109] M. A. Al-Ghouti and D. A. Da'ana, "Guidelines for the use and interpretation of adsorption isotherm models: a review," *Journal of Hazardous Materials*, vol. 393, Article ID 122383, 2020.

[110] I. Langmuir, "The constitution and fundamental properties of solids and liquids. Part I. Solids," *Journal of the American Chemical Society*, vol. 38, no. 11, pp. 2221–2295, 1916.

[111] I. Langmuir, "The constitution and fundamental properties of solids and liquids. II. Liquids," *Journal of the American Chemical Society*, vol. 39, no. 9, pp. 1848–1906, 1917.

[112] I. Langmuir, "The adsorption of gases on plane surfaces of glass, mica and platinum," *Journal of the American Chemical Society*, vol. 40, no. 9, pp. 1361–1403, 1918.

[113] P. U. Shah, N P Raval, M. Vekariya et al., "Adsorption of lead (II) ions onto novel cassava starch 5-choloromethyl-8-hydroxyquinoline polymer from an aqueous medium," *Water Science and Technology*, vol. 74, no. 4, pp. 943–956, 2016.

[114] F Li, D Feng, H Deng et al., "Effects of biochars prepared from cassava dregs on sorption behavior of ciprofloxacin," *Procedia Environmental Sciences*, vol. 31, pp. 795–803, 2016.

[115] H. Freundlich, "Über die Adsorption in Lösungen," *Zeitschrift für Physikalische Chemie*, vol. 57, no. 1, pp. 385–470, 1907.

[116] H. Freundlich, "Kapillarchemie: eine darstellung der chemie der kolloide und verwandter gebiete," *Nature*, vol. 85, no. 2156, pp. 534-535, 1911.

[117] M M. Dubinin and M. Dubinin, "The potential theory of adsorption of gases and vapors for adsorbents with energetically nonuniform surfaces," *Chem. Rev.*vol. 60, no. 2, pp. 235–241, 1960.

[118] M. I. Temkin, "Kinetics of ammonia synthesis on promoted iron catalysts," *Acta Physiochim. URSS*, vol. 12, pp. 327–356, 1940.

[119] P. J. Flory, *Principles of Polymer Chemistry*, Cornell University Press, Ithaca, NY, USA, 1953.

[120] M. Hill and N. London, "Proceedings of the physiological society," *Measurement*, vol. 16, p. 17, 1953.

[121] G. Halsey, H. S. Taylor, and S. Taylor, "The adsorption of hydrogen on tungsten powders," *The Journal of Chemical Physics*, vol. 15, no. 9, pp. 624–630, 1947.

[122] D. S. Jovanović, "Physical adsorption of gases - II: practical application of derived isotherms for monolayer and multilayer adsorption," *Kolloid-Zeitschrift Zeitschrift Für Polym*, vol. 235, pp. 1214–1225, 1969.

[123] S. Brunauer, P. H Emmett, E H. Teller, Emmett, and E. Teller, "Adsorption of Adsorption of Gases in Multimolecular Layersases in multimolecular layers," *J. Am. Chem. Soc.*vol. 60, no. 2, pp. 309–319, 1938.

[124] O. Redlich, D. L Peterson, and L. Peterson, "A useful adsorption isotherm," *J. Phys. Chem.*vol. 63, no. 6, p. 1024, 1959.

[125] J. Toth, "State equation of the solid-gas interface layers," *Acta Chim. Hung.*vol. 69, pp. 311–328, 1971.

[126] R. Sips, "On the structure of a catalyst surface," *The Journal of Chemical Physics*, vol. 16, no. 5, pp. 490–495, 1948.

[127] A. Khan, R. Ataullah, A. Al-Haddad, R. Ataullah, and A. Al-Haddad, "Equilibrium adsorption studies of some aromatic pollutants from dilute aqueous solutions on activated carbon at different temperatures," *Journal of Journal of Colloid and Interface Scienceolloid and Interface Science*, vol. 194, no. 1, pp. 154–165, 1997.

[128] W. Fritz, E Schluender, U. Fritz, and E. U. Schluender, "Simultaneous adsorption equilibria of organic solutes in dilute aqueous solutions on activated carbon," *Chemical Engineering Science*, vol. 29, no. 5, pp. 1279–1282, 1974.

[129] M. Baudu, G. Guibaud, D. Raveau, and P. Lafrance, "Prévision de l'adsorption de molécules organiques en solution aqueuse en fonctions de quelques caractéristiques physico-chimiques de charbons actifs," *Water Quality Research Journal*, vol. 36, no. 4, pp. 631–657, 2001.

[130] W. J Weber, B van Vliet, M J. Weber, and B. M. van Vliet, "Synthetic adsorbents and activated carbons for water treatment: statistical analyses and interpretations," *Journal - American Water Works Association*, vol. 73, no. 8, pp. 426–431, 1981.

[131] A. W. Marczewski, "Basics of liquid adsorption," pp. 11–24, 2002, https://www.adsorption.org.

[132] S. K. Lagergren, "About the theory of so-called adsorption of soluble substances," *Sven. Vetenskapsakad. Handingarl*, vol. 24, pp. 1–39, 1898.

[133] Y. Ho, G McKay, S. Ho, and G. McKay, "The sorption of lead (II) ions on peat," *Water Water Researchesearch*, vol. 33, no. 2, pp. 578–584, 1999.

[134] S. Y. Elovich and O. G. Larinov, "Theory of adsorption from solutions of non-electrolytes on solid (I) equation adsorption from solutions and the analysis of its simplest form, (II) verification of the equation of adsorption isotherm from solutions," *Izv. Akad. Nauk. SSSR, Otd. Khim. Nauk*, vol. 2, no. 2, pp. 209–216, 1962.

[135] A. G. Ritchie and G. Ritchie, "Alternative to the Elovich equation for the kinetics of adsorption of gases on solids," *Journal of the Chemical Society, Faraday Transactions 1: Physical Chemistry in Condensed Phases*, vol. 73, pp. 1650–1653, 1977.

[136] A. Özer, "Removal of Pb (II) ions from aqueous solutions by sulphuric acid-treated wheat bran," *Journal of Hazardous Materials*, vol. 141, no. 3, pp. 753–761, 2007.

[137] G. E. Boyd, A W. Adamson, L. S. Myers, A. W. Adamson, and L. S. Myers, "The The Exchange Adsorption of Ions from Aqueous Solutions by Organic Zeolites. II. Kinetics[1]xchange adsorption of ions from aqueous solutions by organic zeolites. II. Kinetics," *Journal of the American Chemical Society*, vol. 69, no. 11, pp. 2836–2848, 1947.

[138] T. Furusawa, J. M. Smith, and M. Smith, "Fluid—Fluid-Particle and Intraparticle Mass Transport Rates in Slurriesarticle and intraparticle mass transport rates in slurries," *Industrial & Engineering Chemistry Fundamentals*, vol. 12, no. 2, pp. 197–203, 1973.

[139] A. P. Mathews and W. Weber, "Effects of external mass transfer and intraparticle diffusion on adsorption rates in slurry reactors AIChE Symposium Series," vol. 73, no. 166, 1977.

[140] A. L. Hines and R. N. Maddox, *Mass Transfer: Fundamentals and Applications*, Vol. 434, Prentice-Hall, , Englewood Cliffs, NJ, USA, 1985.

[141] W. J Weber, J Morris, C J. Weber, and J. C. Morris, "Kinetics of Kinetics of Adsorption on Carbon from Solutiondsorption on carbon from solution," *Journal of the Sanitary Engineering Division*, vol. 89, no. 2, pp. 31–59, 1963.

[142] R. Leyva-Ramos, C. Geankoplis, and J. Geankoplis, "Model simulation and analysis of surface diffusion of liquids in porous solids," *Chemical Chemical Engineering Sciencengineering Science*, vol. 40, no. 5, pp. 799–807, 1985.

[143] J. Halévy, "La Juive. Opéra en cinq actes de Scribe," *Musique de F. Halévy. Divertissement de M. Taglioni*, 1885.